Chapter 4

Atmospheric Models

4.1 Angular momentum and Hadley Cell

Exercise 30   –   Angular momentum and Hadley Cell

Consider a zonally symmetric circulation (i.e., one with no longitudinal variations) in the atmosphere. In the inviscid upper troposphere one expects such a flow to conserve absolute angular momentum, i.e.,
$$\frac{DA}{Dt} = 0,$$

where A is the absolute angular momentum per unit mass (parallel to the Earth's rotation axis)

$$A = r\left(u + \Omega r\right) = \Omega a^2 \cos^2 \varphi + ua \cos \varphi \quad .$$

Ω is the Earth rotation rate, u the eastward wind component, $r = a \cos \varphi$ is the distance from the rotation axis, a the Earth's radius, and φ latitude.

1. Show, for inviscid zonally symmetric flow, that the relation $\frac{DA}{Dt} = 0$ is consistent with the zonal component of the equation of motion (using our standard notation, with F_x the
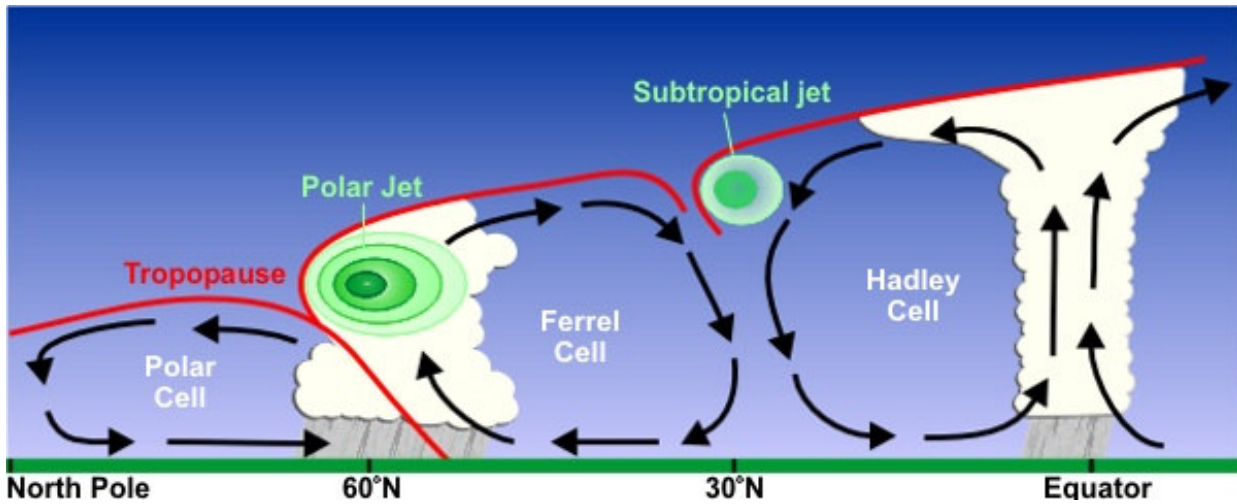
Figure 4.1: Cross section of the subtropical and polar jet streams by latitude.

x-component of the friction force per unit mass)

$$\frac{Du}{Dt} - fv = -\frac{1}{\rho}\frac{\partial p}{\partial x} + F_x$$

in (x, y, z) coordinates, where $y = a\varphi$.

2. Use angular momentum conservation to describe how the existence of the Hadley circulation explains the existence of both the subtropical jet in the upper troposphere.

   Hint: In the upper troposphere, the flow leaves the rising branch of the Hadley cell at the equator (cf. Fig. 4.2) with angular momentum density $A_0 = \Omega a^2$, if we assume that the flow rises from the ground there with no relative motion. The zonal flow can then be described as $u = \Omega a \sin^2 \varphi / \cos \varphi$. Show that the zonal flow will be greatest at the edge of the cell, where φ is greatest, thus producing the subtropical jet.

   Note that $\Omega a^2 = \frac{2\pi}{86400\,s} \cdot (6.371 \cdot 10^6 m)^2 = 3 \cdot 10^9 m^2 s^{-1}$.

3. Describe the near-surface trade winds by recognizing that this low-level flow is under the influence of surface friction and A will therefore be progressively reduced. Show that

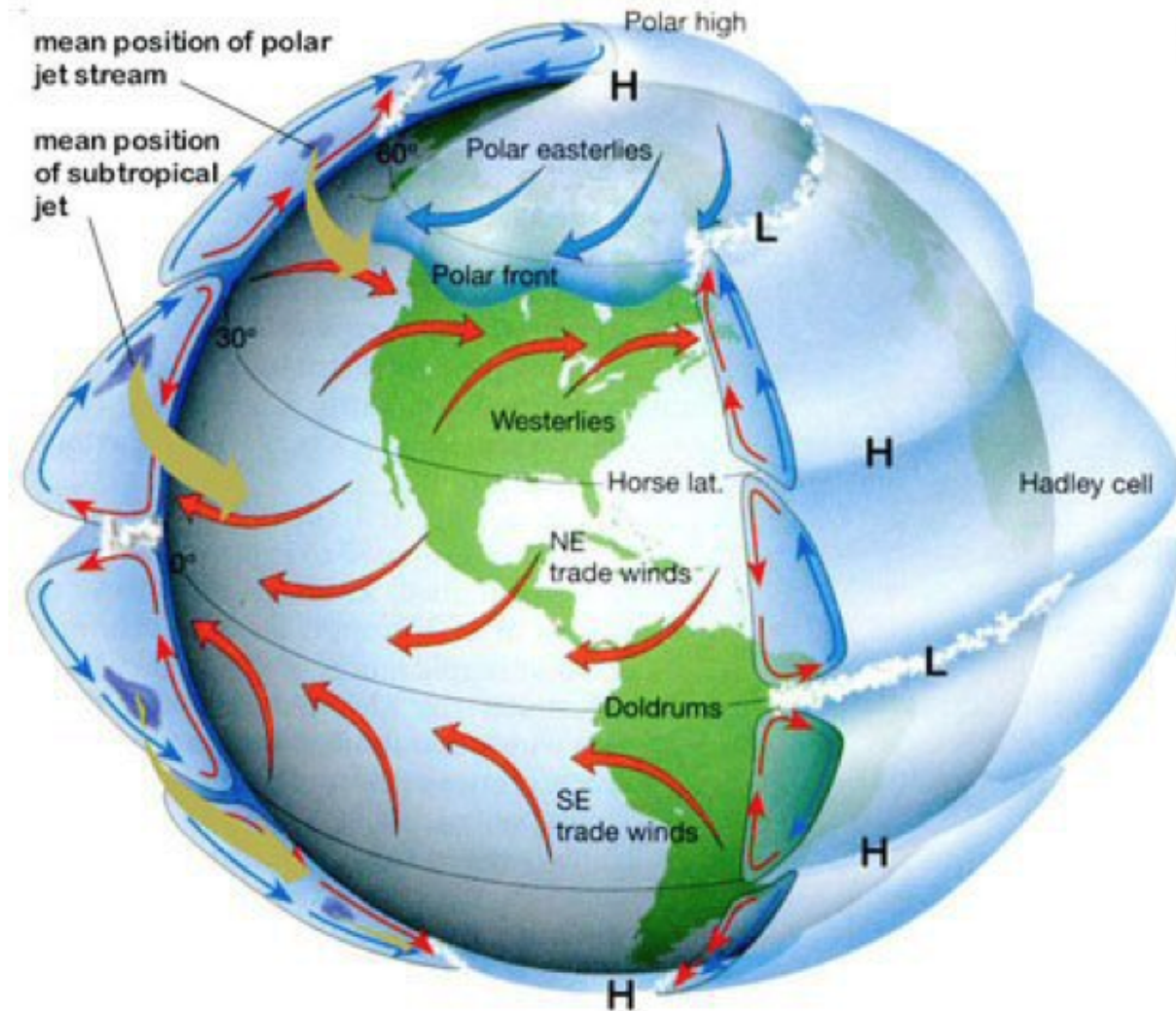$$u_{low} < \Omega a \frac{\sin^2 \varphi}{\cos \varphi}$$

Figure 4.2: Schematic picture of the Hadley Cell and the jet streams. Subtropical jet forms at the poleward limit of the tropical Hadley cell and to first order this circulation is symmetric with respect to longitude. Tropical air rises to the tropopause, and moves poleward before sinking; this is the Hadley cell circulation. As it does so it tends to conserve angular momentum, since friction with the ground is slight. Air masses that begin moving poleward are deflected eastward by the Coriolis force (true for either hemisphere), which for poleward moving air implies an increased westward component of the winds (note that leftward deflection in the southern hemisphere).

and some φ that u_{low} becomes negative (eastward winds).

4. If the Hadley circulation is symmetric about the equator, and its edge is at $20°$ latitude, determine the strength of the subtropical jet.

   (The observed zonal winds are weaker than the value. In reality, non-axisymmetric atmospheric eddies act to reduce angular momentum in the outflow, and hence reduce the strength of the jets.)

5. Consider the tropical Hadley circulation in northern winter. The circulation rises at $10°S$, moves northward across the equator in the upper troposphere, and sinks at $20°N$. Assuming that the circulation, outside the near-surface boundary layer, is zonally symmetric (independent of x) and inviscid (and thus conserves absolute angular momentum about the Earth's rotation axis), and that it leaves the boundary layer at $10°S$ with zonal velocity u = 0, calculate the zonal wind in the upper troposphere and provide the numbers for the equator, $10°N$, and $20°N$.

Solution of Exercise 30

1. For inviscid axisymmetric flow, conservation of angular momentum implies

$$D_t(\Omega a^2 \cos^2 \varphi + ua \cos \varphi) = 0$$

Remember that $y = a\varphi$, $dx = a \cos \varphi \, d\lambda$. Here, we reformulate the planetary term:

$$
\begin{align}
D_t(\Omega a^2 \cos^2 \varphi) &= v\partial_y(\Omega a^2 \cos^2 \varphi) \tag{4.1}\\
&= \Omega av\partial_\varphi(\cos^2 \varphi) \tag{4.2}\\
&= -2\Omega av \sin \varphi \cos \varphi \tag{4.3}\\
&= -fv \cdot a \cos \varphi \tag{4.4}
\end{align}
$$

Similar
$$D_t(ua \cos \varphi) = a \cos \varphi D_t u + u \cdot v \, \partial_\varphi \cos \varphi \tag{4.5}$$

where in the coordinate system

$$D_t u = (\partial_t + u\partial_x + v\partial_y)u + \frac{uv}{a}\tan\varphi \qquad (4.6)$$

(the last term is a metric term). Therefore and under the assumption $\partial_x p = 0$:

$$D_t u - fv = 0 \qquad (4.7)$$

2. Use angular momentum conservation to describe how the existence of the Hadley circulation explains the existence of both the subtropical jet in the upper troposphere. In the upper troposphere, the flow leaves the rising branch of the Hadley cell at the equator (cf. Fig. 4.2) with angular momentum density $A_0 = \Omega a^2$, if we assume that the flow rises from the ground there with no relative motion. We have

$$A = \Omega a^2 \cos^2\varphi + ua\cos\varphi = A_0 = \Omega a^2$$

and therefore the zonal flow can then be described as

$$u = \Omega a \sin^2\varphi / \cos\varphi .$$

The zonal flow will be greatest at the edge of the cell, where φ is greatest, thus producing the subtropical jet.

3. If the return flow, in the lower troposphere, were inviscid and thus also conserved angular momentum with $A_{low} = A_0$, then at a given latitude the low level flow would be the same as that aloft, since in u is a function of φ only. However, in reality this low-level flow is under the influence of surface friction and A will therefore be progressively reduced. Thus,

$$A_{low} = \Omega a^2 \cos^2\varphi + u_{low}a\cos\varphi < A_0 = \Omega a^2$$

$$\text{Thus} \quad u_{low} < \Omega a \frac{\sin^2 \varphi}{\cos \varphi}$$

and some φ_0 north of the equator that u_{low} becomes negative (eastward winds), and so the low level flow will be equatorward and eastward there. (Note that $\Omega a^2 = \frac{2\pi}{86400\,s} \cdot (6.371 \cdot 10^6 m)^2 = 3 \cdot 10^9 m^2 s^{-1}$.)

4. Assume the Hadley circulation is symmetric about the equator, and its edge is at $20°$ latitude, determine the strength of the subtropical jet by

$$u(20°) = \Omega a \sin^2(20°)/\cos(20°) = 57.6\, m\, s^{-1}$$

The observed zonal winds are weaker than the value. In reality, non-axisymmetric atmospheric eddies act to reduce angular momentum in the outflow, and hence reduce the strength of the jets.

5. Consider the angular momentum $A = \Omega a^2 \cos^2 \varphi + ua \cos \varphi = A_0 = \Omega a^2$ with $A_0 = \Omega a^2 \cos^2(10°S) = 2.952 \cdot 10^9 m^2 s^{-1}$.

$$\text{Therefore} \quad u = \frac{A_0 - \Omega a^2 \cos^2 \varphi}{a \cos \varphi}$$

At $\varphi = 0°, u = -13.9\, ms^{-1}$, at $\varphi = 10°, u = 0\, ms^{-1}$, at $\varphi = 20°, u = 42.8\, ms^{-1}$.

4.2 Engery balance model

Energy balance models (EBM) are highly simplified systems of the climate system. A zero-dimensional model of the radiative equilibrium of the Earth is

$$(1 - \alpha)S\pi R^2 = 4\pi R^2 \epsilon \sigma T^4 \tag{4.8}$$

where the left hand side represents the incoming energy from the Sun (the disk) the right hand side represents the outgoing energy from the Earth (the globe), calculated from the Stefan-Boltzmann law assuming a constant radiative temperature, T, that is to be found, and S is the solar constant - the incoming solar radiation per unit area– about $1367 W m^{-2}$, α is the Earth's average albedo, measured to be 0.3. R is Earth's radius = 6.371×10^6 m, σ is the Stefan-Boltzmann constant = $5.67 \times 10^{-8} J K^{-4} m^{-2} s^{-1}$, and ϵ is the effective emissivity of earth (about 0.612). The geometrical constant πR^2 can be factored out, giving

$$(1 - \alpha)S = 4\epsilon\sigma T^4 \tag{4.9}$$

Solving for the temperature,

$$T = \sqrt[4]{\frac{(1 - \alpha)S}{4\epsilon\sigma}} \tag{4.10}$$

This yields an average earth temperature of **288** K. This is because the above equation represents the effective radiative temperature of the Earth (including the clouds and atmosphere). The use of effective emissivity and albedo account for the greenhouse effect.

Note that S itself stems from effective temperature of the sun is the temperature of a black body with the same luminosity per surface area (FBol) as the star and is defined according to the Stefan-Boltzmann law σT_{eff}^4. Notice that the total (bolometric) luminosity of a star is then $L = 4\pi R2\sigma T_{eff}^4$, where R is the stellar radius. The effective temperature of our Sun is around 5780 K.

Stars have a decreasing temperature gradient, going from their central core up to the atmosphere. The "core temperature" of the Sun-the temperature at the centre of the Sun where nuclear reactions take place-is estimated to be 15,000,000 K The effective (blackbody) temperature of a planet can be calculated by equating the power received by the planet with the power emitted by a blackbody of temperature T.

Take the case of a planet at a distance D from the star, of luminosity L.

Assuming the star radiates isotropically and that the planet is a long way from the star, the power absorbed by the planet is given by treating the planet as a disc of radius r, which intercepts some of the power which is spread over the surface of a sphere of radius D (the distance of the planet from the star).

The average emissivity of the earth is estimated from available data. The emissivities of terrestrial surfaces are all in the range of 0.96 to 0.99 (except for some small desert areas which may be as low as 0.7). Clouds, however, which cover about half of the earth's surface, have an average emissivity of about 0.5 (which must be reduced by the fourth power of the ratio of cloud absolute temperature to average earth absolute temperature) and an average cloud temperature of about 258 K. Taking all this properly into account results in an effective earth emissivity of about 0.64 (earth average temperature 285 K). This simple model determines the effect of changes in solar output or change of earth albedo or effective earth emissivity on average earth temperature. It says nothing, however about what might cause these things to change. Zero-dimensional models do not address the temperature distribution on the earth or the factors that move energy about the earth.

Exercise 31   –   Energy balance

The EMB (4.8) determines the effect on average earth temperature of changes in solar constant or change of albedo or effective earth emissivity. Show: The percent change of the average amount of each parameter, considered independently, to cause a one degree Kelvin change in steady-state average earth temperature is Solar constant 1.4%, Albedo 3.3%, Effective emissivity 1.4% using (4.10).

```
## here is the simple calculation:
alpha=0.3
S=1367
sigma=5.67e-8
epsilon=0.612
T= sqrt(sqrt( (1-alpha ) * S/(4 *epsilon* sigma) ))
T
```

Let us have a closer look onto (4.8). The local radiative equilibrium of the Earth is

$$\epsilon \sigma T^4 = (1 - \alpha) S \cos \varphi \cos \Theta \quad \times 1_{[-\pi/2 < \Theta < \pi/2]}(\Theta) \qquad (4.11)$$

Integration over the Earth surface is

$$\int_{-\pi/2}^{\pi/2} R d\varphi \int_0^{2\pi} R \cos \varphi d\Theta \, \epsilon \sigma T^4 = \int_{-\pi/2}^{\pi/2} R \cos^2 \varphi d\varphi \int_{-\pi/2}^{\pi/2} R \cos \Theta d\Theta \, (1 - \alpha) S$$

$$\epsilon \sigma R^2 \int_{-\pi/2}^{\pi/2} d\varphi \int_0^{2\pi} \cos \varphi d\Theta \, T^4 = (1 - \alpha) S R^2 \underbrace{\int_{-\pi/2}^{\pi/2} d\varphi \cos^2 \varphi}_{\frac{\pi}{2}} \underbrace{\int_{-\pi/2}^{\pi/2} \cos \Theta d\Theta}_{2}$$

$$\epsilon \sigma 4\pi \overline{T^4} = (1 - \alpha) S \, \pi \qquad (4.12)$$

giving a similar formula as (4.10) with the definition for the average

$$\overline{T^4} = \frac{1}{4\pi} \int_{-\pi/2}^{\pi/2} d\varphi \int_0^{2\pi} \cos \varphi d\Theta \quad T^4 \quad .$$

What we really want is the mean of the temperature $\overline{T}$. Therefore, we take the fourth root of (4.11):

$$T = \sqrt[4]{\frac{(1 - \alpha) S \cos \varphi \cos \Theta}{\epsilon \sigma}} \quad \times 1_{[-\pi/2 < \Theta < \pi/2]}(\Theta) \qquad (4.13)$$

and integrate this over the sphere:

$$\overline{T} = \sqrt[4]{\frac{(1 - \alpha) S}{\epsilon \sigma}} \frac{1}{4\pi} \int_{-\pi/2}^{\pi/2} d\varphi \int_{-\pi/2}^{\pi/2} \cos \varphi d\Theta \sqrt[4]{\cos \varphi \cos \Theta}$$

$$\overline{T} = \sqrt[4]{\frac{(1 - \alpha) S}{4\epsilon \sigma}} \frac{\sqrt{2}}{4\pi} \underbrace{\int_{-\pi/2}^{\pi/2} (\cos \varphi)^{5/4} d\varphi}_{1.86} \underbrace{\int_{-\pi/2}^{\pi/2} (\cos \Theta)^{1/4} d\Theta}_{2.70} \qquad (4.14)$$

$$= 0.4\sqrt{2} \sqrt[4]{\frac{(1 - \alpha) S}{4\epsilon \sigma}} = 0.57 \sqrt[4]{\frac{(1 - \alpha) S}{4\epsilon \sigma}} \qquad (4.15)$$

Therefore, $\overline{T} \approx \mathbf{163K}$ is a factor $\mathbf{0.57}$ lower than $\mathbf{288}$ K as stated at (4.8). This zero-dimensional

models do not address the heat capacity and the proper temperature distribution on the earth.

```
## here is the simple calculation:
integrand1 <- function(x) {(cos(x))^(5/4)}
integrand2 <- function(x) {(cos(x))^(1/4)}
a1=integrate(integrand1, lower = -pi/2, upper = pi/2)
a2=integrate(integrand2, lower = -pi/2, upper = pi/2)
a=a1$value*a2$value/(4 * pi) *sqrt(2)
```

Which effective ϵ we would expect then? Basically an $\epsilon = \mathbf{0.065}$ is a factor 10 lower than above

which is unrealistic (see below).

If we calculate the zonal mean of (4.13) by integration at the latitudinal cycles

$$\frac{1}{2\pi} \int_0^{2\pi} d\Theta$$

we have

$$T(\varphi) = \mathbf{0.61} \cdot \sqrt[4]{\frac{(1-\alpha)S}{4\epsilon\sigma}} \quad (\cos\varphi)^{1/4} \tag{4.16}$$

as a function on latitude. Here is the calculation:

```
## here is the simple calculation:
alpha=0.3
S=1367
sigma=5.67e-8
epsilon0=0.612
lat=pi/2/90
phi=c(-89:89)

integrand2 <- function(x) {(cos(x))^(1/4)}
a2=integrate(integrand2, lower = -pi/2, upper = pi/2)
b=a2$value/(2 * pi) *sqrt(2)
T= b*sqrt(sqrt( (1-alpha ) * S/(4*epsilon0* sigma) * (cos(lat*phi))^(1/4) ))
Tc=T -273
plot(phi,Tc,type="l",col="red")

dev.copy(png,'ebm_model.png')
dev.off()
```

What happens here is that the heat capacity of the Earth is neglected. During night, the tem-

perature is zero and there is a a strong non-linearity of the outgoing radiation. Furthermore, the
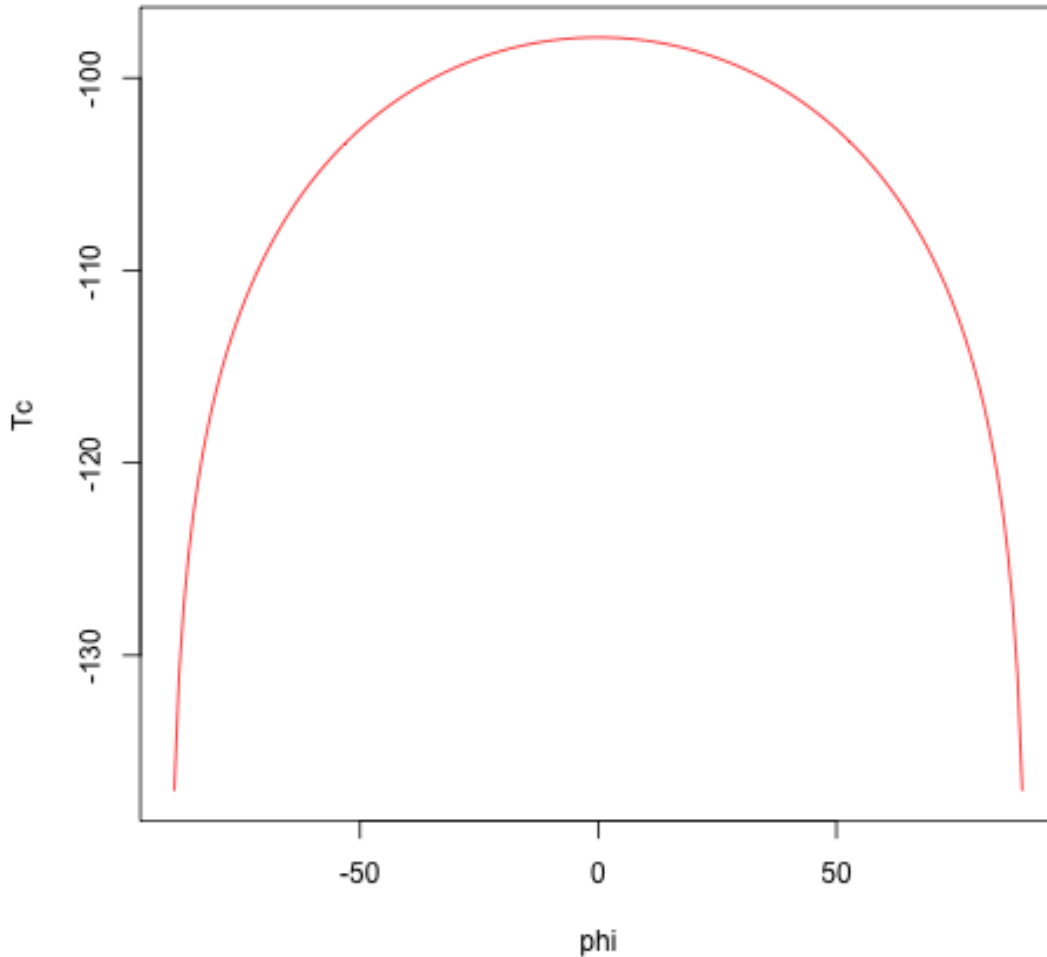
Figure 4.3: Latitudinal temperatures of the EBM with zero heat capacity (4.16).

Earth is a rapidly rotating object. (4.13) can be better used for an object like the moon without an atmosphere, without a significnt heat capacity, and a slowly rotating body. The correct energy balance shall be

$$C_p \, \partial_t T \; = \; (1 - \alpha) S \cos \varphi \cos \Theta \quad \times 1_{[-\pi/2 < \Theta < \pi/2]}(\Theta) \; - \; \epsilon \sigma T^4 \quad . \qquad (4.17)$$

with C_p representing the heat capacity multiplied with the depth of the atmosphere-ocean layer. If we consider the zonal mean and averaged over the diurnal cycle, wecan assume that the heat capacity is mainly given by the ocean. Observational evidence is that the diurnal variation of the ocean surface is in the order of 1-2 K only. The energy balance (4.17) is integrated over the longitude and over the day

$$\tilde{T}(\tilde{t}) = \frac{1}{2\pi} \int_0^{2\pi} T(t)\, d\Theta \quad \text{with} \quad \tilde{T}^4 \approx \frac{1}{2\pi} \int_0^{2\pi} T^4\, d\Theta$$

and therefore

$$C_p\, \partial_{\tilde{t}}\tilde{T} = (1-\alpha)S\cos\varphi \cdot \underbrace{\frac{1}{2\pi} \int_{-\pi/2}^{\pi/2} \cos\Theta\, d\Theta}_{2} - \epsilon\sigma\tilde{T}^4 \tag{4.18}$$

$$= (1-\alpha)\frac{S}{\pi}\cos\varphi - \epsilon\sigma\tilde{T}^4 \; . \tag{4.19}$$

In the following we will drop the tilde sign.

The linearized EBM

Since we know the approximate temperature on Earth, we may linearize (4.13) around $0°C$. It reduces to

$$(1-\alpha)S\cos\varphi\cos\Theta \quad \times 1_{[-\pi/2<\Theta<\pi/2]}(\Theta) = A + BT_C \tag{4.20}$$

where $A = \epsilon\sigma 273^4 K^4 = 193 W/m^2$, $B = \epsilon\sigma 3T^3 273^3 K^3 = 2.1 W/m^2/K$ comes from the Taylor expansion, and T_C is the temperature in °C. Then,

$$A + BT_C = (1 - \alpha)S\cos\varphi \cdot \frac{1}{2\pi}\underbrace{\int_{-\pi/2}^{\pi/2}\cos\Theta\, d\Theta}_{2} \tag{4.21}$$

$$= (1 - \alpha)\frac{S}{\pi}\cos\varphi \tag{4.22}$$

$$T_C = (1 - \alpha)\frac{S}{\pi B}\cos\varphi - \frac{A}{B} \tag{4.23}$$

The global mean is therefore

$$\overline{T_C} = (1 - \alpha)\frac{S}{\pi B}\frac{1}{2}\underbrace{\int_{-\pi/2}^{\pi/2}d\varphi\cos^2\varphi}_{\frac{\pi}{2}} - \frac{A}{B} \tag{4.24}$$

$$= (1 - \alpha)\frac{S}{4B} - \frac{A}{B} \tag{4.25}$$

seen as the green line in Fig. 4.5 with 12.4°C.

```
## here is the simple calculation for the linear model:
alpha=0.3
S=1367
sigma=5.67e-8
epsilon0=0.612
lat=pi/2/90
phi=c(-89:89)
A=epsilon0 * sigma *273^4
A=213

B=epsilon0 *sigma* 3 *  273^3
rhs= 2/(2*pi)* (1-alpha ) * S* cos(lat*phi)
Tc=(rhs- A)/B
plot(phi,Tc,type="l",col="black")

Tm=  ((1-alpha ) * S/(4*B)   -A/B)  * rep(1, 179)
lines(phi,Tm,col="green")

dev.copy(png,'ebm_linear_model.png')
dev.off()
```

In section 4.3 we will explore in detail the influence of meridional transports on temperatures,
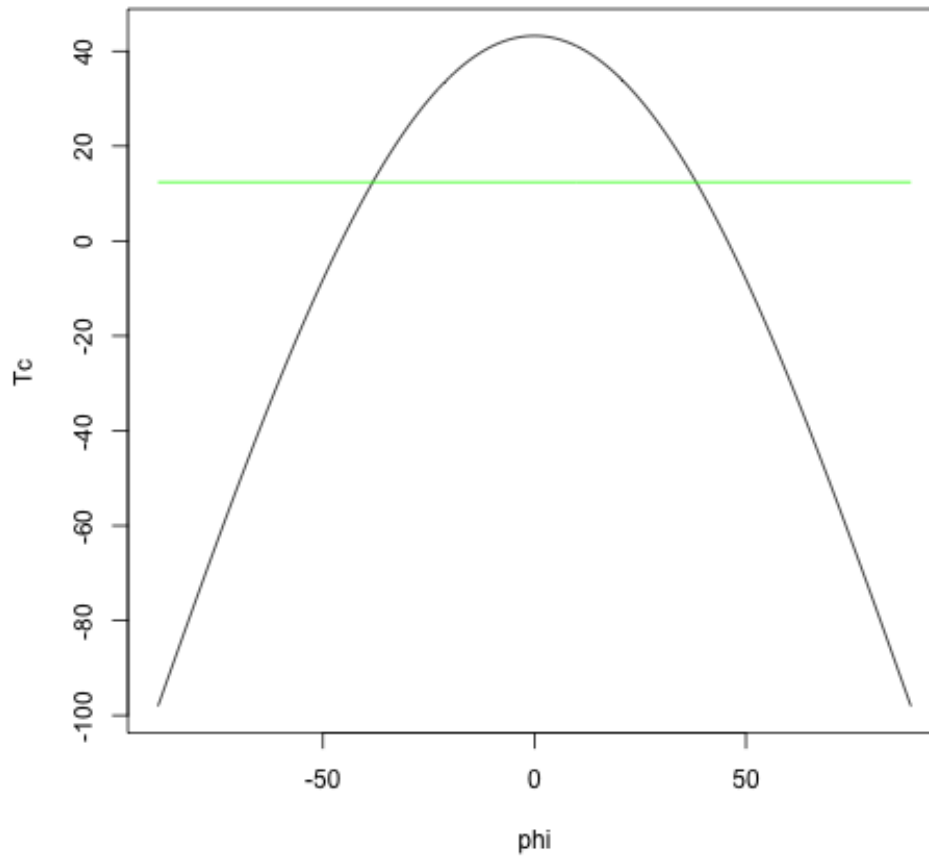
Figure 4.4: Temperatures of the linear EBM: (4.23) in red and (4.33) in green showing the mean. The model has been tuned by the parameter $A = 213W/m^2$.

where the transport is parameterized as diffusion and the radiative fluxes are as in (4.23). Here, we start with a simplfied approach first.

Exercise 32   –   **Analytical EBM**

Solve the vertically integrated energy equation where we include the atmosphere and ocean in

one temperature T and describe the heat transport (sensible, latent and ocean) as diffusion:

$$C_p\,\partial_t T \;=\; k\,\partial_y^2 T \;+\; (1-\alpha)Q_S^{top} - (A + B\,T) \tag{4.26}$$

The albedo $\alpha = 0.3$ is chosen as a fixed parameter, $y = R\varphi$, and

$$Q_S^{top} = \frac{S}{\pi}\cdot\cos\varphi \quad . \tag{4.27}$$

Furthermore, there is no transport across the poles. The gradient at the North and South Pole vanishes:

$$\partial_y T(\varphi = \pm\pi/2) \;=\; 0 \quad . \tag{4.28}$$

Solution

One can separate the dynamics into a gloal mean and a function depending on latitude.

$$\overline{T} \;=\; \frac{1}{2}\int_{-\pi/2}^{\pi/2} T\,d\varphi\,\cos\varphi \tag{4.29}$$

$$T_1 \;=\; T - \overline{T} \tag{4.30}$$

Therefore,
$$C_p\frac{d}{dt}\overline{T} \;=\; (1-\alpha)\frac{S}{2\pi}\int_{-\pi/2}^{\pi/2} d\varphi\,\cos^2\varphi - (A + B\,\overline{T}) \tag{4.31}$$

$$=\; (1-\alpha)\frac{S}{4} - (A + B\,\overline{T}) \tag{4.32}$$

for the global mean with the solution

$$\overline{T}(t) = (1-\alpha)S\,\frac{1}{4B} - \frac{A}{B} \;+\; \overline{T}(t=0)\cdot\exp\!\left(-\frac{B}{C_p}t\right) \tag{4.33}$$

Typical values for C_p are $2\cdot 10^8\,J/m^2/K$.

For T_1 we have

$$C_p \partial_t T_1 = \frac{k}{R^2} \partial_\varphi^2 T_1 + (1-\alpha)S\left(\frac{\cos\varphi}{\pi} - \frac{1}{4}\right) - BT_1 \tag{4.34}$$

$$= \left[\frac{k}{R^2}\partial_\varphi^2 - B\right]T_1 + (1-\alpha)S\left(\frac{\cos\varphi}{\pi} - \frac{1}{4}\right) \tag{4.35}$$

Because of the boundary condition (4.28), the solution for T_1 must have the form $a_l \cos(l\varphi)$

$$T_1 = \sum_{l=1}^{\infty} a_l \cos(l\varphi) + C \tag{4.36}$$

For the homogenous part of (4.35), we have

$$\frac{d}{dt}a_l = -\left[\frac{\frac{kl^2}{R^2} + B}{C_p}\right]a_l \tag{4.37}$$

$$a_l = \exp\left(-\left[\frac{\frac{kl^2}{R^2} + B}{C_p}\right]t\right) \tag{4.38}$$

For the inhomogenous part, we are seeking for a particular solution for (4.35):

$$T_1^p = a_1 \cos\varphi + C \tag{4.39}$$

and therefore

$$0 = \left[\frac{k}{R^2}\partial_\varphi^2 - B\right](a_1\cos\varphi + C) + (1-\alpha)\frac{S}{\pi}\cdot\cos\varphi - (1-\alpha)\frac{S}{4} \tag{4.40}$$

giving two conditions

$$0 = \left[-\frac{k}{R^2} - B\right]a_1 + (1-\alpha)\frac{S}{\pi} \tag{4.41}$$

$$0 = -BC - (1-\alpha)\frac{S}{4} \tag{4.42}$$

and can calulate the constants

$$a_1 \;=\; (1-\alpha)\frac{S}{\pi}\left[\frac{k}{R^2}+B\right]^{-1} \tag{4.43}$$

$$C \;=\; -(1-\alpha)\frac{S}{4B} \tag{4.44}$$

to get finally

$$T_1 = (1-\alpha)\frac{S}{\pi}\left[\frac{k}{R^2}+B\right]^{-1}\cos\varphi - (1-\alpha)\frac{S}{4B} + \sum_{l=2}^{\infty} a_l \cos(l\varphi) \tag{4.45}$$

The equilibrium solution is therefore

$$T_{eq} = \lim_{t\to\infty} T = -\frac{A}{B} + (1-\alpha)\frac{S}{\pi}\left[\frac{k}{R^2}+B\right]^{-1}\cos\varphi \tag{4.46}$$

```
## here is the calculation for the 1 dim energy balance model:
alpha=0.3
S=1367
sigma=5.67e-8
epsilon0=0.612
lat=pi/2/90
phi=c(-89:89)

A=epsilon0 * sigma *273^4
A=213
r=40.0e6/(2*pi)
k=1*r^2
B=epsilon0 *sigma* 3 *  273^3
km= k/r^2 +B
Amod=A - (1-alpha ) * S/4  *(k/r^2)/km

rhs2= 1/(pi)* (1-alpha ) * S* cos(lat*phi) /B
Tc2=  - A/B + rhs2
plot(phi,Tc2,type="l",col="red")

rhs= 1/(pi)* (1-alpha ) * S* cos(lat*phi)  *(k/r^2 +B)^(-1)
Tc=  - Amod/B + rhs
lines(phi,Tc,type="l",col="blue")
Tm=  ((1-alpha ) * S/(4*B)  -A/B)  * rep(1, 179)
lines(phi,Tm,col="green")

dev.copy(png,'ebm_linear_1d_model.png')
dev.off()
```
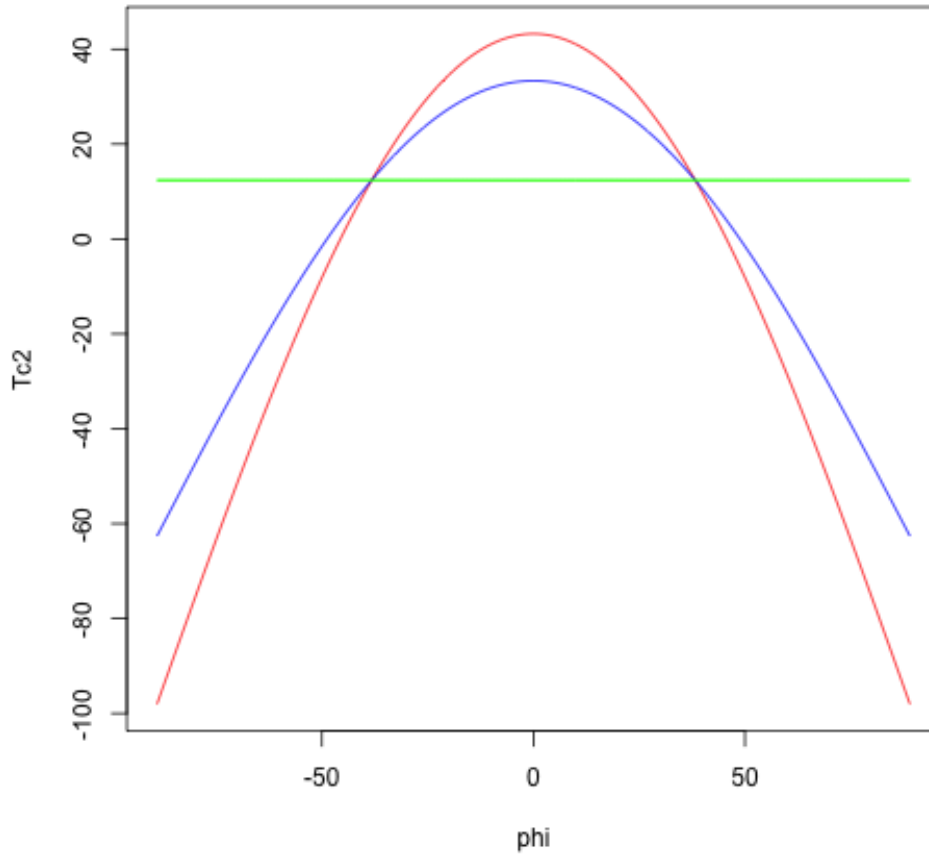
Figure 4.5: Temperatures of the linear EBM: (4.23) in red and (4.33) in green showing the mean with no diffusion. The new one-dimensional model (4.46) is in blue. The model has been tuned by the parameter A to give the same mean temperature (see code). Maximum and minimum temperatures for red are at 43°C and -98°C, whereas for blue are for 33°C and -63°C, respectively.

As a logical next step, we now integrate the non-linear energy balance numerically.

$$C_p \, \partial_t T \;=\; k \, \partial_y^2 T \;+\; (1 - \alpha) \frac{S}{\pi} \cos \varphi \;-\; \epsilon \sigma T^4 \quad . \tag{4.47}$$

Exercise 33   –   Numerical solution of 1D EBM

- Calculate the one-dimensional EBM using differnt time steps

- Identify / extract the finite difference scheme which is used approximate the 2nd derivative

- Run the program and play with the parameters (heat capacity, diffusion coefficient).

```r
# EBM_EulerForward.R
# 1D diffusion EBM equation, explicit scheme

alpha=0.3
S=1367
sigma=5.67e-8
epsilon0=0.612
lat=pi/2/90
phi=c(-90:90)
cp=4.2e6 *1 # cp_water = 4.6e3; rho_water=1e3; h=1m
r=40.0e6/(2*pi)
tabs=272
ddx=40.0e6/360
coslat=cos(phi *lat)
k=(1.5e6 + 2.5e6 * coslat)  # in m^2/s
knorm=1.5e6* rep(1, 181)


plot(phi,k,type="l",col="red", main = "Diffusion",xlim = c(-90, 90),  ylim = c(0, 4.1
lines(phi,k/2,type="l",col="blue")
lines(phi,knorm,type="l",col="green")
dev.copy(png,'Diffusion_ebm_1d.png')
dev.off()

#Constants
L.X<-179 #width of lattice
L.T<-5000000  #length of time
dx <- ddx    #space step in m
dt <- 1000 #time step in s
D<-  k           #Diffusion coefficent
globini=270  # initial condition
N.x<-L.X + 2   #number of space boxes + 2 boundary boxes
N.t<-L.T/dt       #number of time boxes

dtc=dt/cp
dtcdx=dtc/(dx^2)
dtdx=dt/(dx^2)
cfl=dtdx*max(D)  # CFL criterium, this number shall be smaller than 0.5

T<-matrix(globini,N.t,N.x)    #grid
Transport <-matrix(0,N.t,N.x)

#temporary vector which stores the state of of one timestep:
T.temp<-rep(globini,N.x)
Transport.temp<-rep(0,N.x)
```

```
#Set the starting and boundary condition, here one value in the middle:
T[1,N.x/2]<- globini

for (n in 1:(N.t-1))
{
  for (j in 2:(N.x-1))
  {
    sw=(1-alpha)*S/pi *coslat[j]
    lw=epsilon0*sigma * T.temp[j]^4
    T.temp[j]<-T[n,j]+D[j]*dtdx*(T[n,j+1]-2*T[n,j]+T[n,j-1])+dtc*(sw -lw)
    Transport.temp[j]=cp*D[j]*(T[n,j+1]-T[n,j])/ddx * 40.e6*coslat[j]
  }
  T.temp[1] <- T.temp[2]
  T.temp[N.x] <- T.temp[N.x-1]
  Transport.temp[1]=0
  Transport.temp[N.x]=0
  T[n+1,]<-T.temp
  Transport[n+1,]=Transport.temp
}

filled.contour((1:N.t)*dt/1e6,phi,T-tabs,
        color.palette=rainbow,xlab="time",ylab="latitude")

dev.copy(png,'ebm_nonlinear_1d_num.png')
dev.off()

filled.contour((1:N.t)*dt/1e6,phi,Transport*1e-15,
        color.palette=rainbow,xlab="time",ylab="latitude")

dev.copy(png,'Transport_ebm_nonlinear_1d_num.png')
dev.off()
#---
# plot equilibrium
A=epsilon0 * sigma *273^4
A=213
r=40.0e6/(2*pi)
k=1*r^2
B=epsilon0 *sigma* 3 *  273^3
km= k/r^2 +B
Amod=A - (1-alpha ) * S/4  *(k/r^2)/km
rhs2= 1/(pi)* (1-alpha ) * S* cos(lat*phi) /B
Tc2=  - A/B + rhs2
plot(phi,Tc2,type="l",col="black")

lines(phi,T[N.t,]-tabs,type="l",col="red")
max(T[N.t,]-tabs)

dev.copy(png,'End_ebm_nonlinear_1d_num.png')
dev.off()
```
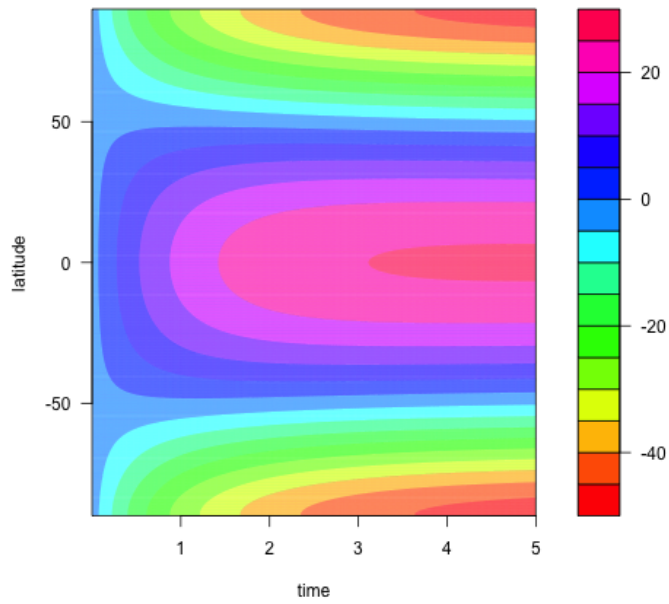
Figure 4.6: Temperature evolution of the one dimensional EBM: Units are °C.
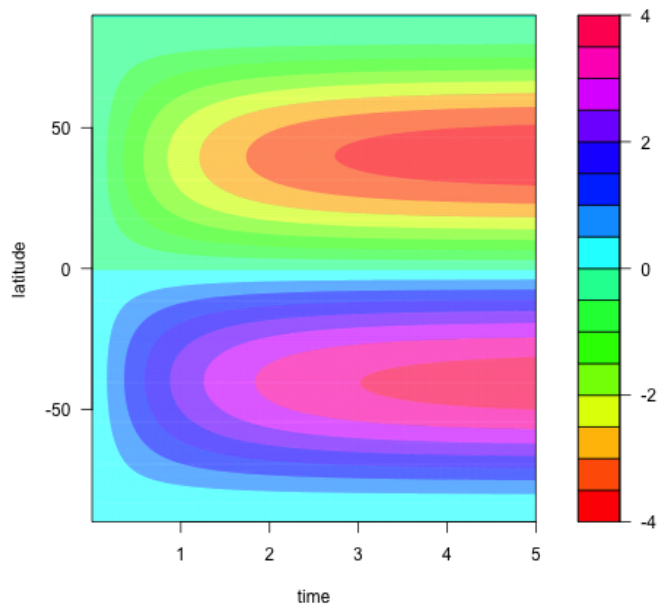

Figure 4.7: Time evolution of the northward meridional heat transport in PW $= 10^{15}$ W.
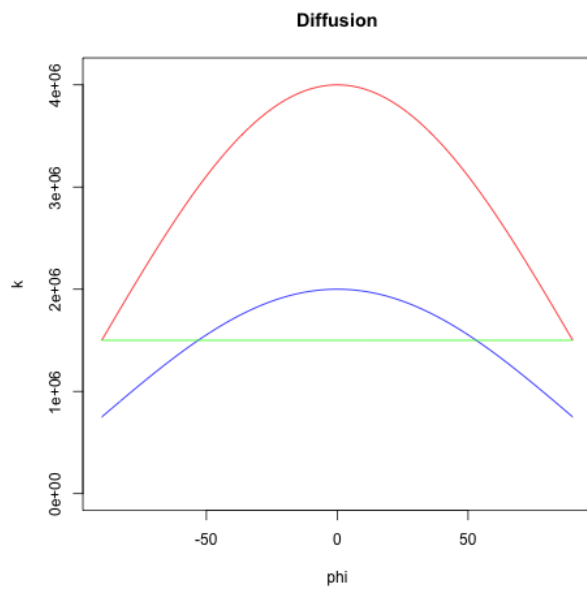
Figure 4.8: Diffusion coefficients for different versions of the model (m^2/s). Exercise 33.
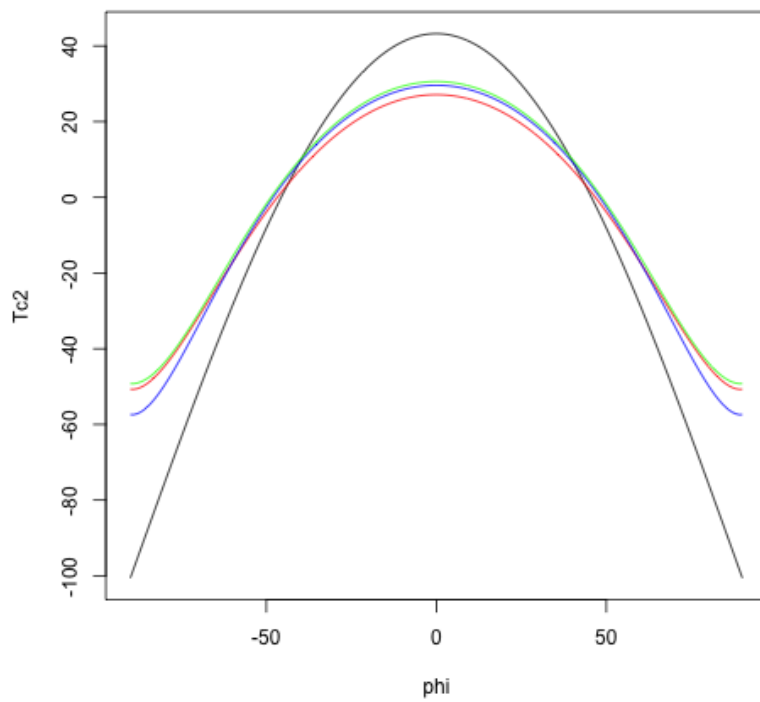
Figure 4.9: Equilibrium temperature in °C. The solutions are related to the diffusion coefficients as displayed in Fig. 4.8. Black: Analytical solution for the linearized model (4.46).

Exercise 34 – **Analytical EBM: Ice-albedo feedback**

Based in exercise 32, one can introduce a climate-dependent formulation of the planetary albedo α on the global temperature:

$$\alpha(T) = \alpha_0 - \alpha_1 \cdot \overline{T} \tag{4.48}$$

a) Solve the Energy balance model (4.26) for the case $\alpha(\overline{T})$ as in (4.48).

b) Show that the stability of the solution depends on certain parameters (like α_1).

c) Explain the ice-albedo effect through this solution!

Exercise 35 – **Analytical EBM: Budyko**

In exercise 32, the transport is parameterized as diffusion. Here, we simplfy the approach:

$$C_p \, \partial_t T \;=\; -k \, (T - \overline{T}) \;+\; (1-\alpha) Q_S^{top} - (A + B \, T) \tag{4.49}$$

Task: Solve the Energy balance model.

Solution

One can separate the dynamics into a gloal mean $\overline{T}(t)$ and a function T_1 depending on latitude.

$$\overline{T}(t) = (1-\alpha)S \, \frac{1}{4B} \; - \; \frac{A}{B} \;+\; \overline{T}(t=0) \cdot \exp\left(-\frac{B}{C_p} t\right) \tag{4.50}$$

For T_1 we have

$$T_1 = (1-\alpha)\frac{S}{\pi}\frac{1}{k+B} \, \cos\varphi - (1-\alpha)\frac{S}{4B} + \sum_{l=2}^{\infty} a_l \cos(l\varphi) \tag{4.51}$$

The equilibrium solution is therefore

$$T_{eq} = \lim_{t\to\infty} T \;=\; -\frac{A}{B} \;+\; (1-\alpha)\frac{S}{\pi}\frac{1}{k+B} \cos\varphi \tag{4.52}$$

Ice-albedo feedback

For Q_S, one needs a climate-dependent formulation of the planetary albedo α, which can be parameterized in terms of the temperature:

$$\alpha(T) = 0.42 - 0.20 \cdot \tanh\left[0.052\left(T - 276.15K\right)\right] \qquad . \qquad (4.53)$$

This parameterization incorporates high albedos of snow and ice in terms of the surface temperature (T in Kelvin).

```R
# EBM_EulerForward.R
# 1D diffusion EBM equation, explicit scheme
S=1367
sigma=5.67e-8
epsilon0=0.612
lat=pi/2/90
phi=c(-90:90)
cp=4.2e6 *1 # cp_water = 4.6e3; rho_water=1e3; h=1m
r=40.0e6/(2*pi)
tabs=272
ddx=40.0e6/360
coslat=cos(phi *lat)
k=(1.5e6 + 2.5e6 * coslat)  # in m^2/s

#Constants
L.X<-179 #width of lattice
L.T<-50000000  #length of time
dx <- ddx    #space step in m
dt <- 1000 #time step in s
D<-  k           #Diffusion coefficent

globini=270
N.x<-L.X + 2    #number of space boxes + 2 boundary boxes
N.t<-L.T/dt        #number of time boxes

dtc=dt/cp
dtcdx=dtc/(dx^2)
dtdx=dt/(dx^2)
cfl=dtdx*max(D)  # CFL criterium, this number shall be smaller than 0.5

T<-matrix(globini,N.t,N.x)    #grid
Transport <-matrix(0,N.t,N.x)

#temporary vector which stores the state of of one timestep:
T.temp<-rep(globini,N.x)
Transport.temp<-rep(0,N.x)
```

```
#Set the starting and boundary condition, here one value in the middle:
T[1,N.x/2]<- globini

for (n in 1:(N.t-1))
{
  for (j in 2:(N.x-1))
  {
    alpha=0.42 -  0.20 * tanh(0.052* ( T[n,j] - 276.15 ))
    sw=(1-alpha)*S/pi *coslat[j]
    lw=epsilon0*sigma * T.temp[j]^4
    T.temp[j]<-T[n,j]+D[j]*dtdx*(T[n,j+1]-2*T[n,j]+T[n,j-1])+dtc*(sw -lw)
    Transport.temp[j]=cp*D[j]*(T[n,j+1]-T[n,j])/ddx * 40.e6*coslat[j]
  }
  T.temp[1] <- T.temp[2]
  T.temp[N.x] <- T.temp[N.x-1]
  Transport.temp[1]=0
  Transport.temp[N.x]=0
  T[n+1,]<-T.temp
  Transport[n+1,]=Transport.temp
}

filled.contour((1:N.t)*dt/1e6,phi,T-tabs,
        color.palette=rainbow,xlab="time",ylab="latitude")

dev.copy(png,'ebm_nonlinear_1d_alb.png')
dev.off()

filled.contour((1:N.t)*dt/1e6,phi,Transport*1e-15,
        color.palette=rainbow,xlab="time",ylab="latitude")

#dev.copy(png,'Transport_ebm_nonlinear_1d_alb.png')
#dev.off()
#---
# plot equilibrium
A=epsilon0 * sigma *273^4
alpha=0.3
A=213
r=40.0e6/(2*pi)
k=1*r^2
B=epsilon0 *sigma* 3 *  273^3
km= k/r^2 +B
Amod=A - (1-alpha ) * S/4  *(k/r^2)/km
rhs2= 1/(pi)* (1-alpha ) * S* cos(lat*phi) /B
Tc2=  - A/B + rhs2
plot(phi,Tc2,type="l",col="black")

lines(phi,T[N.t,]-tabs,type="l",col="red")
max(T[N.t,]-tabs)

dev.copy(png,'End_ebm_nonlinear_1d_alb.png')
dev.off()
```
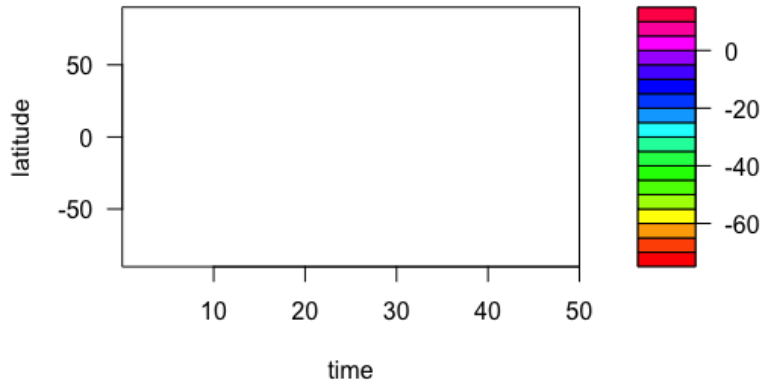
Figure 4.10: As Fig. 4.6, but including the ice-albedo feedback and a low initial condition.
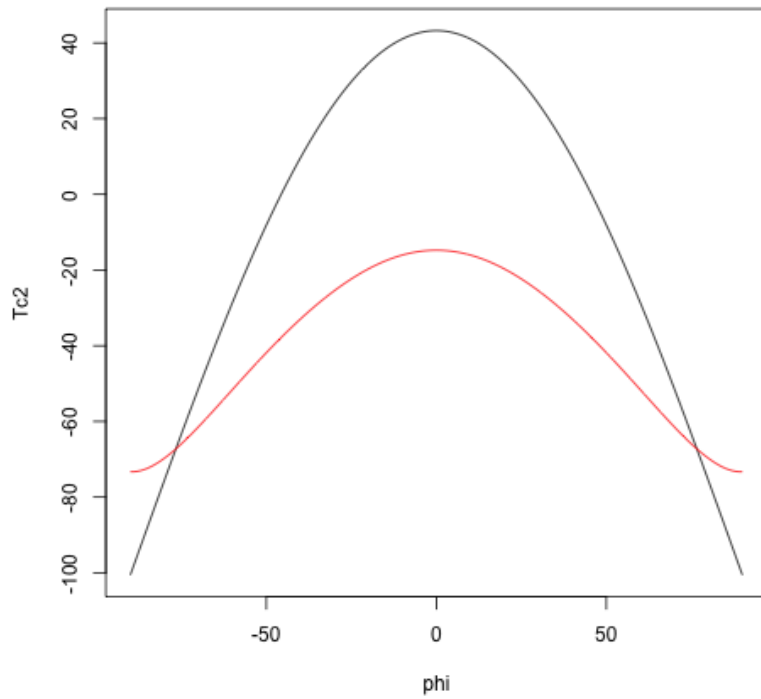

Figure 4.11: As Fig. 4.9, but including the ice-albedo feedback and a low initial condition.

4.3   Moist atmospheric energy balance model*

The model considers a zonally and annually averaged circulation of the atmosphere and calculates surface fresh water fluxes and surface heat fluxes along with sea surface temperatures. The EBM treats the transport processes as diffusion. The balances of energy will be used to derive equations for the atmospheric temperature and fresh water flux. The thermodynamic equation (internal plus potential energy) in the atmosphere in isobaric coordinates reads

$$C_p \left[\partial_t T_a + \nabla \cdot (v\, T_a) + \partial_p(\omega T_a) \right] = \partial_p Q_R + Q_L + \partial_p Q_S + \frac{R T_a}{p} \omega \qquad (4.54)$$

where v and ∇ are the horizontal vector of wind and the gradient operator, T_a atmospheric temperature, p pressure, $\omega = \frac{d}{dt} p$ vertical wind, and C_p specific heat at constant pressure $(1004\, J\, kg^{-1}\, K^{-1})$. Q_R and Q_S are the radiative and sensible heat fluxes, respectively. Q_L denotes the latent heat release due to phase transitions in the air. This term includes condensation of water vapour $(c > 0)$, evaporation of cloud water $(c < 0)$, and evaporation in unsaturated air $(e > 0)$:

$$Q_L = L_v\, (c - e) \qquad (4.55)$$

where L_v is the latent heat of condensation $(L_v = 2.5 \cdot 10^6\, J\, kg^{-1})$.

The last term on the right hand side of equation (4.54) is related to the fact that because pressure decreases with height and air is a compressible fluid, air that rises expands (and air that sinks contracts). Air that expands does work against its surroundings and because of the first law of thermodynamics (conservation of energy) this work needs to be paid for (reduction in temperature). So internal energy is consumed in expanding the parcel of air outwards against the atmosphere (expanding air cools).[1]

---

[1] Furthermore, we can assume an adiabatic process is one where no heat is exchanged with the surroundings. This is a reasonable approximation for typical rising air because other processes like conduction or radiative heat transfer are quite slow. In this context, the potential temperature is introduced. The potential temperature of a parcel of fluid at pressure P is the temperature that the parcel would acquire if adiabatically brought to a standard reference pressure

Additionally to (4.54), the budget equations for the mass mixing ratio of water vapour q_v and cloud water q_w are used:

$$\partial_t q_v + \nabla \cdot (v \, q_v) + \partial_p(\omega \, q_v) = e - c + E \qquad (4.57)$$

$$\partial_t q_w + \nabla \cdot (v \, q_w) + \partial_p(\omega \, q_w) = c - \wp \qquad (4.58)$$

where $\wp$ denotes the formation of precipitation and E denotes the evaporation from the ground (ocean and land).

The budget equations (4.54, 4.57) and (4.58) are now vertically integrated and zonally averaged. It is assumed that in the vertically integrated left hand side of (4.58) the first two terms vanish (stationarity, small horizontal transports). Furthermore, the vertically integrated last term on the right hand side of (4.54) is neglected. With $\omega = 0$ at the top and bottom, (4.58) reduces to

$$\int \frac{dp}{g} c = \int \frac{dp}{g} \wp \qquad , \qquad (4.59)$$

where g is the gravitational acceleration ($9.81 \, m \, s^{-2}$). The net precipitation P on the ground

----

P_0, usually 1000 millibars. The potential temperature is denoted θ and, for air, is often given by

$$\theta = T \left(\frac{P_0}{P} \right)^{R/c_p} , \qquad (4.56)$$

where T is the current absolute temperature (in K) of the parcel, R is the gas constant of air, and c_p is the specific heat capacity at a constant pressure. $R/c_p = 0.286$ for air (meteorology). Potential temperature is a more dynamically important quantity than the actual temperature. This is because it is not affected by the physical lifting or sinking associated with flow over obstacles or large-scale atmospheric turbulence. A parcel of air moving over a small mountain will expand and cool as it ascends the slope, then compress and warm as it descends on the other side- but the potential temperature will not change in the absence of heating, cooling, evaporation, or condensation (processes that exclude these effects are referred to as dry adiabatic). Since parcels with the same potential temperature can be exchanged without work or heating being required, lines of constant potential temperature are natural flow pathways. The equation comes from the enthalpy form of the first law of thermodynamics can be written as: $dh = T \, ds + v \, dp$, where dh denotes the enthalpy change, T the temperature, ds the change in entropy, v the specific volume, and p the pressure. For adiabatic processes, the change in entropy is zero: $dh = v \, dp$. For approximately ideal gases, such as the dry air in the Earth's atmosphere, the equation of state, $pv = RT$ can be substituted by $dpv = R/vdT \frac{dp}{p} = \frac{c_p}{R} \frac{dT}{T}$, where the $dh = c_p dT$ was used and both terms were divided by the product pv. Integrating yields 4.56.

$(p = p_0 = 10^5 N m^{-2} = 1000\, mb)$ is defined as

$$P = \int \frac{dp}{g} \, (\wp - e) \quad .$$
(4.60)

This yields the vertically integrated balances for the mixing ratio of water vapour and atmospheric temperature:

$$\int \frac{dp}{g} \, \partial_t(C_p T_a) + \int \frac{dp}{g} \nabla \cdot (C_p v T_a) = Q_R^{top} - Q_R^{bottom} + L_v\, P + Q_S^{bottom}$$

$$\int \frac{dp}{g} \, \partial_t(L_v q_v) + \int \frac{dp}{g} \nabla \cdot (L_v v q_v) = L_v\, (E - P) \quad .$$
(4.61)

The one dimensional atmosphere EBM prognoses the vertically integrated mixing ratio of water vapour and atmospheric temperature along with (4.61).[2] This yields one vertically integrated energy equation:

$$C\, \partial_t T_A + \int \frac{dp}{g} \nabla \cdot (C_p v T_a) + \int \frac{dp}{g} \nabla \cdot (L_v v q) = Q_R^{top} - F_{oa}$$
(4.62)

where $F_{oa} = Q_R^{bottom} - L_v E - Q_S^{bottom}$ denotes the ocean-atmosphere heat flux calculated by bulk formulas. The net radiation on top of the atmosphere Q_R^{top} is the difference between net solar radiation and net outgoing longwave radiation Q_{LW}^{top}. In a further approximation, the longwave radiation Q_{LW}^{top} canbe described by a linear law $A + BT$ (4.20). A climate-dependent formulation of the planetary albedo α, in terms of the surface air temperature was given in (4.53). With equation (4.62) the surface temperature T_A is calculated prognostically, while the fresh water flux for the ocean surface is given by the right hand side of equation (4.61) by evaluating the left hand side of the water vapour budget.

Meridional Transports

The transport parameterizations are based on diffusion. The mechanism of heat and moisture trans-

---

[2]To evaluate the effective change of the vertically integrated humidity and temperature in equations (4.61), the height distribution of humidity and temperature must be taken into account using an empirical relation between the lapse rate and surface temperature β_1, β_2: $C\, \partial_t T_A = (C_p \beta_1 + L_v \beta_2)\, \partial_t T_A$

port in middle and high latitudes by baroclinic instability is the most important mechanism in the atmospheric energy balance model. Consider an atmospheric condition with isotherms coincident with latitude circles. A cold anomaly, which could be thought of as a cold air outbreak from the North American continent, results in a changed surface heat flux from the ocean. In the region of strong temperature gradient, cyclones (low pressure) and anticyclones (high pressure on the northern hemisphere) are formed. These traveling weather systems move north-eastward defining the major storm track. The scale over which this process is important is about 1000 km.

This process is the main source of meridional heat transport in middle and high latitudes. The balances of heat and moisture (4.61) are averaged over a length scale of synoptic scale disturbances of O(1000) km and a time scale longer than the life time of such disturbances (e.g. two weeks). The variables can be splitted into a large-scale, long-term quantities ($\overline{T_a}, \overline{q_v}, \overline{v}$) and the deviations ($T_a', q_v', v'$). The moments $\overline{v'T_a'}$ and $\overline{v'q_v'}$ are connected mainly with transient processes in the atmosphere. The transients act as diffusion in a statistical sense bringing warm and moist air poleward due to individual high and low pressure contributions.

The eddy fluxes, in a statistically steady state of the atmosphere, scale as:

$$\overline{v'T_a'} \sim \left(\frac{\partial \overline{T_a}}{\partial y} \right) \tag{4.63}$$

where T', v' are the perturbation of potential temperature and meridional velocity. The vertical integrated sensible eddy heat transport can be calculated in terms of the surface temperature gradient T_A

$$\int \frac{dp}{g} \ \ \overline{v'T_a'} \ = \ - \ K_s \ \left(\frac{\partial \, T_A}{\partial y} \right) \qquad . \tag{4.64}$$

where K_s is tuned to reproduce the current climate.

The latent eddy heat transport is parameterized as

$$\overline{v'q_v'} \ = \ rh(p) \ \frac{\partial \, q_s}{\partial \overline{\overline{T_a}}}(\overline{T_a}, p) \ \ \overline{v'T_a'} \ , \tag{4.65}$$

where rh is the relative humidity and q_s the saturation water vapour. The relative humidity is prescribed. For the latent heat transport (4.65), the relative humidity and $\frac{\partial q_s}{\partial T}$ strongly decrease with height. Therefore, the surface values for the latent heat transport is a good choice in the vertical integrated model:

$$\int \frac{dp}{g} \; \overline{v'q'_v} \;\; = \;\; -K_l \quad rh(p_0) \quad \frac{\partial q_s}{\partial T_A}(T_A, p_0) \quad \left(\frac{\partial T_A}{\partial y} \right) \qquad . \qquad (4.66)$$

As for the sensible heat transport, the coefficient K_l can be tuned that (4.66) reproduces the latent eddy heat transports of current climate. The eddy activity is greatly enhanced over the ocean surfaces as opposed to over land surfaces. In the Northern Hemisphere, two major storm tracks exists extending northeast across the Atlantic and Pacific oceans from the east coast of the major continents. It is along these tracks that the majority of eddy heat and vorticity transport takes place. In the Southern Hemisphere the transport is relatively homogeneous in the zonal direction.[3] In the boxmodel in section 6, we assume that the atmospheric heat transport across the box boundaries are completely by transient eddies.

---

[3]The heat transport by stationary baroclinic waves is larger in winter on the northern hemisphere when the land-sea contrast is most pronounced. Green **?** argued that stationary eddies are more transient phenomena which repeatedly occur at the same location. This happens due to fixed topographic effects providing perturbations upon which baroclinic waves can grow. These phenomena relating to stationary eddies are ultimately driven by the large scale baroclinicity of the atmosphere. Therefore, standing eddies could be parameterized as transient eddies.

Chapter 5

Ocean Circulation

5.1 Wind-driven ocean circulation

What drives the ocean currents? At first, we might answer, the winds drive the circulation. But if we think more carefully about the question, we might not be so sure. We might notice, for example, that strong currents, such as the North Equatorial Countercurrents in the Atlantic and Pacific Ocean go upwind. Spanish navigators in the 16th century noticed strong northward currents along the Florida coast that seemed to be unrelated to the wind. How can this happen? And, why are strong currents found offshore of east coasts but not offshore of west coasts?[1]

Friction is essential for the transfer of momentum in a fluid. Friction transfers momentum from the atmosphere to the ocean through the thin, frictional, Ekman layer at the sea surface. Friction transfers momentum from the ocean to the solid earth through the Ekman layer at the sea floor. Friction along the sides of subsea mountains leads to pressure differences on either side of the mountain which causes another kind of drag called *form drag*. This is the same drag that causes

---

[1]Answers to the questions can be found in a series of three remarkable papers published from 1947 to 1951. In the first, Harald Sverdrup (1947) showed that the circulation in the upper kilometer or so of the ocean is directly related to the curl of the wind stress. Henry Stommel (1948) showed that the circulation in oceanic gyres is asymmetric because the Coriolis force varies with latitude. Finally, Walter Munk (1950) added eddy viscosity and calculated the circulation of the upper layers of the Pacific. Together the three oceanographers laid the foundations for a modern theory of ocean circulation.

wind force on cars moving at high speed. In the vast interior of the ocean, however, the flow is frictionless, and vorticity is conserved. Such a flow is said to be *conservative*. Here, we apply the vorticity dynamics for the ocean and include the wind stress term in (3.39, 3.40):

$$D_t u - fv \;=\; -\frac{1}{\rho}\frac{\partial p}{\partial x} + \frac{1}{\rho}\partial_z \tau_{xz} \tag{5.1}$$

$$D_t v + fu \;=\; -\frac{1}{\rho}\frac{\partial p}{\partial y} + \frac{1}{\rho}\partial_z \tau_{yz} \tag{5.2}$$

in order to get the modified vorticity balance (3.61):

$$\frac{D}{Dt}(\zeta + f) - \frac{(\zeta + f)}{h}\frac{D}{Dt}h \;=\; \frac{1}{\rho}\,\mathrm{curl}_z\,\partial_z \tau \;=\; \frac{1}{\rho}\left(\frac{\partial}{\partial x}\partial_z \tau_{yz} - \frac{\partial}{\partial y}\partial_z \tau_{xz}\right) \tag{5.3}$$

The formulation 'wind stress curl' stands for the z-component of

$$\nabla \times \begin{pmatrix} \tau_x \\ \tau_y \\ 0 \end{pmatrix} = curl \begin{pmatrix} \tau_x \\ \tau_y \\ 0 \end{pmatrix} \quad .$$

Exercise 36 – **Non-dimensional vorticity dynamics including wind stress**

a) Derive the the non-dimensional version of the vorticity equation (5.3) assuming that h is not varying and include friction! We can vertically integrate (5.3) over depth $\int_{-D}^{0} dz$:

$$\frac{D}{Dt}(\zeta + f) \;=\; A_H \nabla^2 \zeta + \frac{1}{\rho D}\left(\frac{\partial}{\partial x}\tau_y - \frac{\partial}{\partial y}\tau_x\right) \quad . \tag{5.4}$$

Include the Reynolds number $Re = UL/A_H$, Rossby number $Ro = U/(f_0 L)$, and the wind stress strength number $\alpha = \tau_0 L/(\rho_0 D U^2)$. *Compare to exercises 4, 26.*

b) Estimate the order of magnitude of the characteristic numbers for the ocean ! You can use Table 5.1.

	Quantity	Ocean
horizontal velocity	U	$1.6 \cdot 10^{-2}\, ms^{-1}$
horizontal length	L	$10^6\, m$
vertical length	D	$10^3\, m$
wind stress	τ_0	$1.5 \cdot 10^{-1}\, Pa$
Coriolis parameter at 45°N	$f_0 = 2\Omega \sin \varphi_0$	$10^{-4}\, s^{-1}$
density	ρ_0	$10^3\, kgm^{-3}$
viscosity (turbulent)	A_H	$10^2 - 10^4\, m^2 s^{-1}$
Reynolds number	Re	$1.6 - 160$
wind stress strength number	α	$1 \cdot 10^3$

Table 5.1: Table shows the typical scales in the ocean system for exercise 36.

Solution of Non-dimensional vorticity dynamics including wind stress

Starting from (5.4),

$$\frac{1}{T}\frac{D}{Dt_d}\left(\frac{1}{T}\zeta_d + f_0 f_d\right) = A_H \frac{1}{L^2 T}\nabla_d^2 \zeta_d + \frac{\tau_0}{\rho_0 DL}\left(\frac{\partial}{\partial x_d}\tau_{y,d} - \frac{\partial}{\partial y_d}\tau_{x,d}\right) \quad (5.5)$$

$$\frac{D}{Dt_d}\left(\frac{1}{T}\zeta_d + f_0 f_d\right) = A_H \frac{1}{L^2}\nabla_d^2 \zeta_d + \frac{\tau_0 T}{\rho_0 DL}\left(\frac{\partial}{\partial x_d}\tau_{y,d} - \frac{\partial}{\partial y_d}\tau_{x,d}\right) \quad .(5.6)$$

Multiplying with T and using $T = L/U$, we obtain

$$\frac{D}{Dt_d}\left(\zeta_d + \frac{f_0 L}{U} f_d\right) = \frac{A_H}{UL}\nabla_d^2 \zeta_d + \frac{\tau_0 L}{\rho_0 DU^2}\left(\frac{\partial}{\partial x_d}\tau_{y,d} - \frac{\partial}{\partial y_d}\tau_{x,d}\right) \quad (5.7)$$

and finally

$$\frac{D}{Dt_d}\left(\zeta_d + \frac{1}{Ro} f_d\right) = \frac{1}{Re}\nabla_d^2 \zeta_d + \alpha \left(\frac{\partial}{\partial x_d}\tau_{y,d} - \frac{\partial}{\partial y_d}\tau_{x,d}\right) \quad (5.8)$$

5.1.1 Sverdrup relation

Suppose for simplicity that h is constant, so the only 'topography' is that of the spherical shape
of the ocean. This produces a simple version of the vorticity balance in the ocean circulation, the

Sverdrup relation. For most regions, the right hand side in (5.3) or the left hand side in (5.8) is dominated by the term $v\partial_y f = v\beta$.

$$v\beta = \frac{1}{\rho}\left(\frac{\partial}{\partial x}\partial_z\tau_{yz} - \frac{\partial}{\partial y}\partial_z\tau_{xz}\right) \quad. \tag{5.9}$$

Integrating over z, we receive

$$\beta\int_h^0 dz\, v = \beta V = \frac{1}{\rho}\mathrm{curl}_z\,\tau(z=0) = \frac{1}{\rho}\left(\frac{\partial\tau_{yz}}{\partial x} - \frac{\partial\tau_{xz}}{\partial y}\right) \quad. \tag{5.10}$$

Mass transport and Stream Lines of Sverdrup's Theory*

While Sverdrup was analyzing observations of equatorial currents, he derived the relation by the the wind stress to mass transport within the upper ocean. It is assumed that the flow is stationary, that lateral friction and molecular viscosity are small, that non-linear terms such as $u\partial u/\partial x$ are small. With these assumptions, the horizontal components of the momentum equation are:

$$\frac{\partial p}{\partial x} = f\,\rho\,v + \frac{\partial\tau_{\mathrm{xz}}}{\partial z} \tag{5.11}$$

$$\frac{\partial p}{\partial y} = -f\,\rho\,u + \frac{\partial\tau_{\mathrm{yz}}}{\partial z} \tag{5.12}$$

Sverdrup integrated these equations from the surface to a depth $-D$ equal to or greater than the depth at which the horizontal pressure gradient becomes zero. We can define

$$\frac{\partial P}{\partial x} = \int_{-D}^0 \frac{\partial p}{\partial x}\,dz, \qquad \frac{\partial P}{\partial y} = \int_{-D}^0 \frac{\partial p}{\partial y}\,dz, \tag{5.13}$$

M_x, M_y are the mass transports in the wind-driven layer extending down to an assumed depth of no motion:

$$M_x \equiv \int_{-D}^0 \rho\,u\,(z)\,\,dz, \qquad M_y \equiv \int_{-D}^0 \rho\,v\,(z)\,\,dz \quad. \tag{5.14}$$

The horizontal boundary condition at the sea surface is the wind stress, and the boundary at depth $-D$ is zero stress because the currents go to zero:

$$\tau_{xz}(0) \;=\; \tau_x \qquad \tau_{xz}(-D) = 0 \tag{5.15}$$

$$\tau_{yz}(0) \;=\; \tau_y \qquad \tau_{yz}(-D) = 0 \quad . \tag{5.16}$$

Using these definitions and boundary conditions, (5.11, 5.12) becomes:

$$\frac{\partial P}{\partial x} \;=\; f\,M_y + \tau_x \tag{5.17}$$

$$\frac{\partial P}{\partial y} \;=\; -f\,M_x + \tau_y \quad . \tag{5.18}$$

In a similar way, Sverdrup integrated the continuity equation over the same vertical depth, assuming the vertical velocity at the surface and at depth $-D$ are zero, to obtain:

$$\frac{\partial M_x}{\partial x} + \frac{\partial M_y}{\partial y} = 0 \tag{5.19}$$

Differentiating (5.17) with respect to y and (5.18) with respect to x, subtracting, and using (5.19) gives:

$$\beta\,M_y \;\;=\;\; \frac{\partial \tau_y}{\partial x} - \frac{\partial \tau_x}{\partial y} = \mathrm{curl}_z(\tau) \tag{5.20}$$

$$\text{where} \quad \beta \equiv \frac{\partial f}{\partial y} = \frac{2\Omega\cos\varphi}{R} \tag{5.21}$$

with R as earth's radius and φ as latitude. Over much of the open ocean, the wind is zonal and $\partial \tau_y / \partial x$ is sufficiently small that

$$M_y \approx -\frac{1}{\beta}\frac{\partial \tau_x}{\partial y} \tag{5.22}$$

Substituting (5.22) into (5.19), and (5.21) we obtain

$$\frac{\partial M_x}{\partial x} = -\frac{1}{2\,\Omega\,\cos\varphi}\left(\frac{\partial \tau_x}{\partial y}\tan\varphi + \frac{\partial^2 \tau_x}{\partial y^2}R\right) \tag{5.23}$$
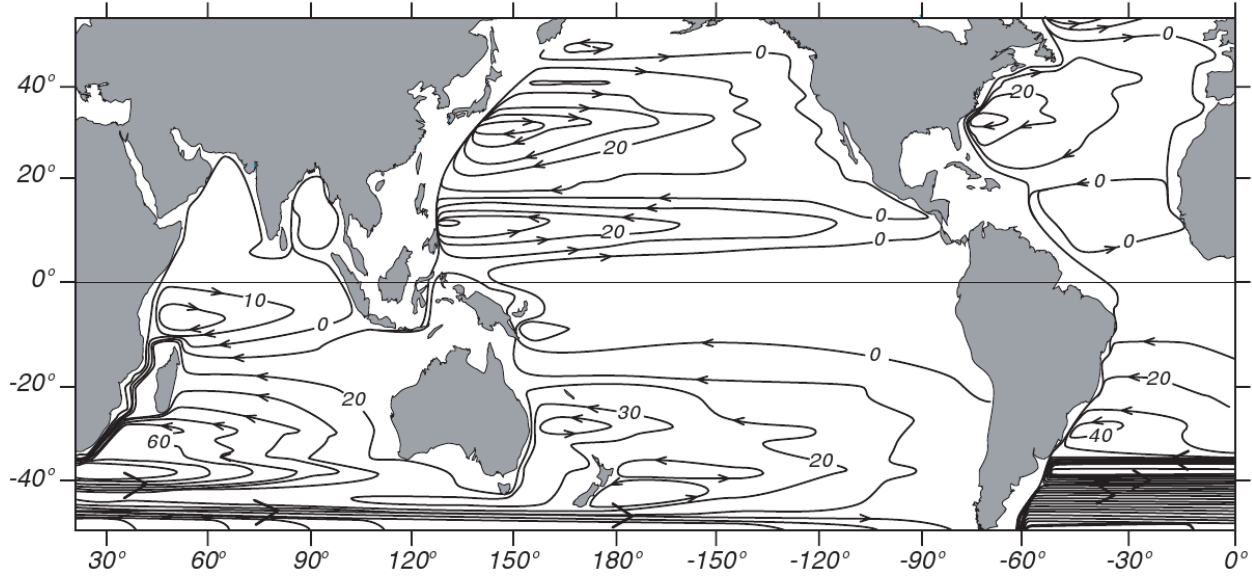
Figure 5.1: Depth-integrated Sverdrup transport applied globally using the wind stress from Hellerman and Rosenstein (1983). Contour interval is **10** Sverdrups (Tomczak and Godfrey, 1994).

Sverdrup integrated this equation from a north-south eastern boundary at $x = 0$, assuming no flow into the boundary. This requires $M_x = 0$ at $x = 0$. Then

$$M_x = -\frac{1}{2\,\Omega\,\cos\varphi}\left(\left[\int_0^x \frac{\partial\tau_x}{\partial y}dx'\right]\tan\varphi + \left[\int_0^x \frac{\partial^2\tau_x}{\partial y^2}dx'\right]R\right) \tag{5.24}$$

$$= -\frac{1}{2\,\Omega\,\cos\varphi}\left(\tan\varphi\,\frac{\partial}{\partial y}\left[\int_0^x \tau_x dx'\right] + R\,\frac{\partial^2}{\partial y^2}\left[\int_0^x \tau_x dx'\right]\right) \quad . \tag{5.25}$$

If τ_x can be approximated by its zonal mean, then

$$M_x = -\frac{\Delta x}{2\,\Omega\,\cos\varphi}\left[\tan\varphi\,\frac{\partial\langle\tau_x\rangle}{\partial y} + R\,\frac{\partial^2\langle\tau_x\rangle}{\partial y^2}\right] \tag{5.26}$$

where Δx is the distance from the eastern boundary of the ocean basin, and brackets indicate zonal averages of the wind stress.

5.1.2 Ekman Pumping

Ekman Pumping in a thin Ekman layer

Let us come now to the wind-driven forcing at the surface, the Ekman Pumping. The pressure terms are small because the Ekamn layer is thin. The Ekman layer near the surface of the ocean extends only about 10-20 meters deep[2]. The Ekman transports V_E, U_E describe the dynamics in the upper mixed layer:

$$fV_E = -\tau_x/\rho \tag{5.27}$$

$$fU_E = \tau_y/\rho \tag{5.28}$$

where $U_E = \int_{-E}^{0} u\,dz$ and $V_E = \int_{-E}^{0} v\,dz$ are the depth-integrated velocities in the thin friction-dominated Ekman layer at the sea surface. The vertical velocity at the surface is zero and denote w_E as the Ekman vertical velocity the bottom of the Ekman layer.

$$-\int_{-E}^{0} \frac{\partial w}{\partial z}dz = w_E = \frac{\partial}{\partial x}U_E + \frac{\partial}{\partial y}V_E \tag{5.29}$$

The curl of the wind stress τ produces a divergence of the Ekman transports leading to a vertical velocity w_E at the bottom of the Ekman layer.

$$w_E = \text{curl}\left(\frac{\tau}{\rho\,f}\right) = \frac{\partial}{\partial x}\left(\frac{\tau_y}{\rho\,f}\right) - \frac{\partial}{\partial y}\left(\frac{\tau_x}{\rho\,f}\right) \quad . \tag{5.30}$$

The order of magnitude of the Ekman vertical velocity w_E can be estimated as from a typical wind stress variation of $0.2 Nm^{-2}$ per 2000 km in y-direction:

$$w_E \simeq -\frac{\Delta\tau_x}{\rho\,f_0\Delta y} \simeq \frac{1}{10^3 kgm^{-3}}\frac{0.2Nm^{-2}}{10^{-4}s^{-1}\,2\cdot10^6 m} \simeq 32\,\frac{m}{yr} \tag{5.31}$$

---

[2]The instrumentation sensitive enough to observe a velocity profile in such a shallow depth has only been available since around 1980. Also, wind waves modify the flow near the surface, and make observations close to the surface rather difficult.

See for a scetch see Fig. 5.2. The center of a subtropical gyre is a high pressure zone. Circulation around the high pressure is clockwise in the northern hemisphere and counterclockwise in the southern hemisphere, due to the Coriolis effect. The high pressure in the center is due to the westerly winds on the northern side of the gyre and easterly trade winds on the southern side. These cause frictional surface currents towards the latitude at the center of the gyre. This build-up of water in the center creates flow towards the equator in the upper 2 km of the ocean. This flow is returned towards the pole in an intensified western boundary current. The boundary current of the North Atlantic Gyre is the Gulf Stream, of the North Pacific Gyre the Kuroshio Current, etc..

Ekman vertical velocity and vertical geostrophic velocity

The Ekman vertical velocity must be balanced by a vertical geostrophic velocity $w_g \left(z = -E \right)$.

$$w_E = w_g \tag{5.32}$$

Ekman pumping drives a vertical geostrophic current in the ocean's interior. Figure 5.2 is a sketch of the cross section of the region between $10°$N and $60°$N, and it shows the pool of warm water in the upper kilometer centered on $30°$N. Conversely, divergent transports lead to low sea level. The mean north-south pressure gradients associated with the highs and lows are balanced by the Coriolis force of east-west geostrophic currents in the upper ocean. Westerlies in the north drive a southward transport, the trades in the south drive a northward transport. The converging Ekman transports must be balanced by downward geostrophic velocity (5.32).

Figure 5.3 shows the mean zonal winds in the Pacific, together with the north-south Ekman transports driven by the zonal winds. Notice that convergence of transport leads to downwelling, which produces a thick layer of warm water in the upper kilometer of the water column, and high sea level.
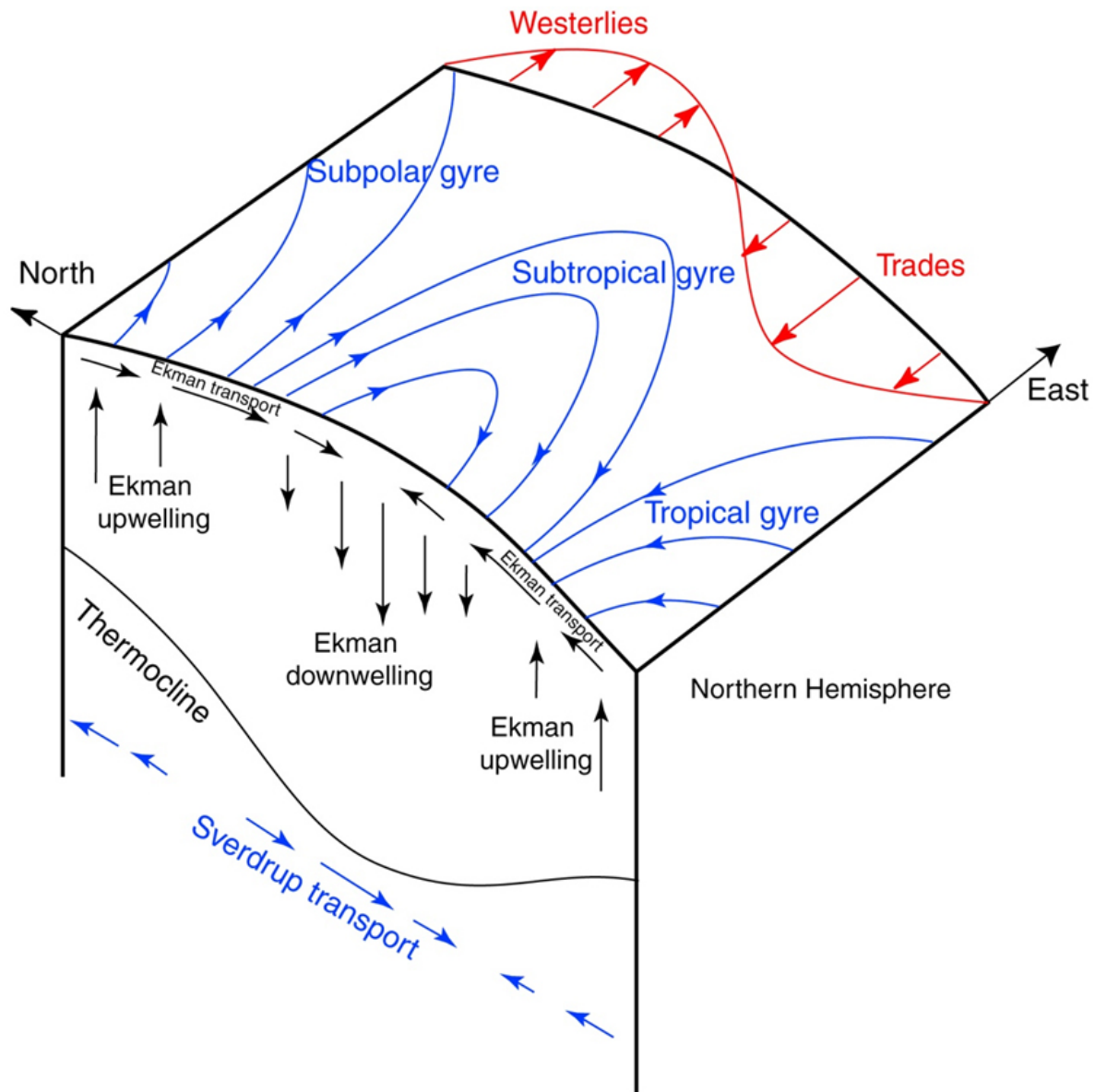
Figure 5.2: Ekman pumping that produces a downward velocity at the base of the Ekman layer forces the fluid in the interior of the ocean to move southward. Winds at the sea surface drive Ekman transports to the right of the wind in this northern hemisphere example. The converging Ekman transports driven by the trades and westerlies drive a downward geostrophic flow just below the Ekman layer.
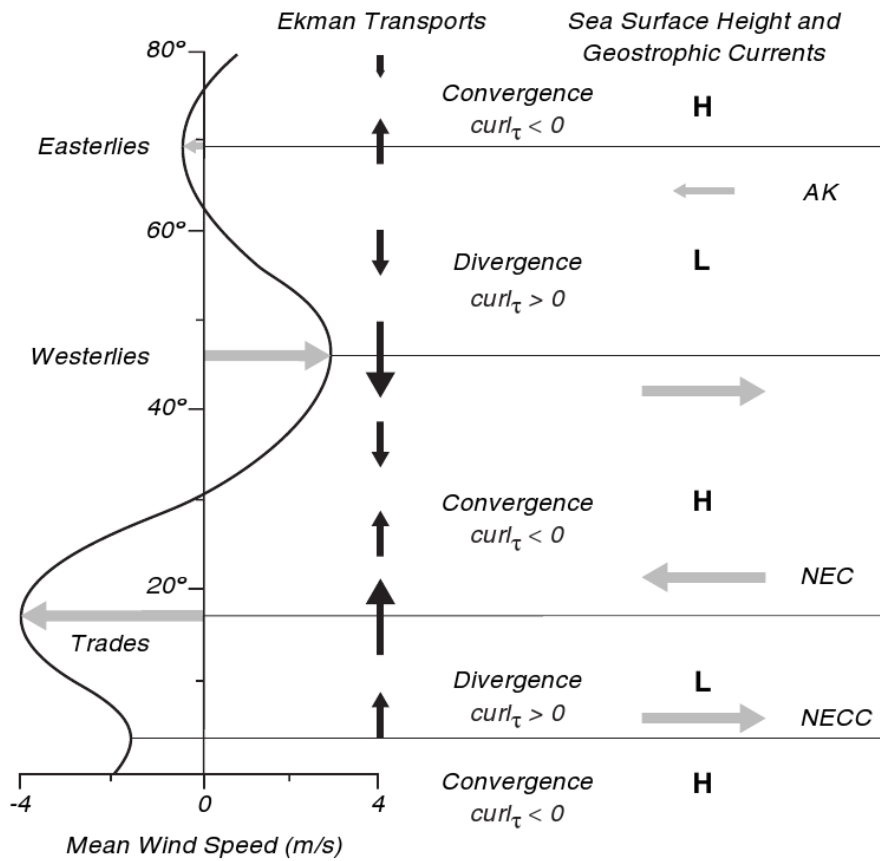
Figure 5.3: Ekman transports due to winds in the north Pacific (left) lead to Ekman pumping (center), which sets up north-south pressure gradients in the upper ocean. The pressure gradients are balanced by the Coriolis force due to east-west geostrophic currents (right). Horizontal lines indicate regions where the curl of the zonal wind stress changes sign. AK: Alaskan Current, NEC: North Equatorial Current, NECC: North Equatorial Counter Current.

Exercise 37   –   Ekman transports and pumping

The Ekman transports V_E, U_E describe the dynamics in the upper mixed layer:

$$fV_E = -\tau_x/\rho_0 \tag{5.33}$$

$$fU_E = \tau_y/\rho_0 \tag{5.34}$$

Derive the Ekman pumping w_E velocity at the bottom of the mixed layer

$$w_E = \text{curl}\left(\frac{\tau}{f\rho_0}\right) = \frac{\partial}{\partial x}\left(\frac{\tau_y}{\rho_0 f}\right) - \frac{\partial}{\partial y}\left(\frac{\tau_x}{\rho_0 f}\right) \quad . \tag{5.35}$$

Exercise 38   –   Sverdrup relation, Ekman transports and pumping

The windstress vector τ is taken zonal. Assume $\tau_x = -\tau_0 \cos \pi y/B$ for an ocean basin $0 < x < L, 0 < y < B$. The wind driven meridional ocean velocity is given by the Sverdrup relation

$$\beta V = \text{curl}(\tau/\rho_0) = -\frac{\partial}{\partial y}\tau_x/\rho_0 \quad . \tag{5.36}$$

1. at what latitudes y are $|V|$ and $|V_E|$ maximum? Calculate their magnitudes. Take constant $f = 10^{-4}$ s^{-1} and $\beta = 1.8 \cdot 10^{-11}$ m^{-1}s^{-1} and $B = 5000$ km, $\tau_0/\rho_0 = 10^{-4}$ m^{2}s^{-2}.

2. Calculate the maximum of w_E for constant f (value see above). Is this measurable?
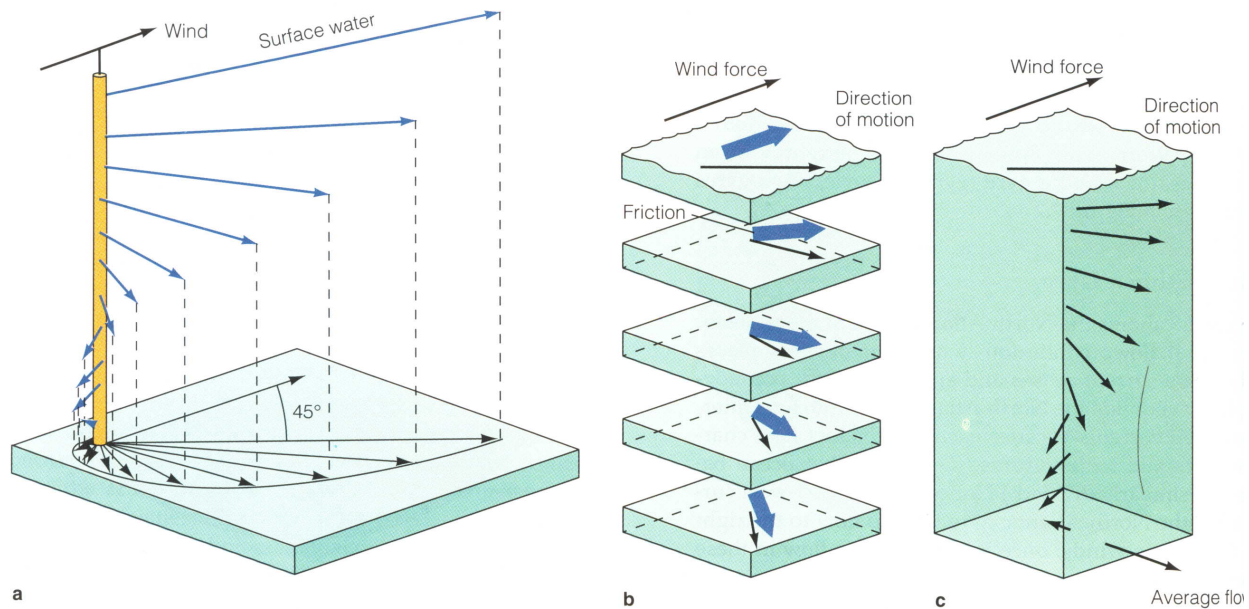
Figure 5.4: The Ekman spiral and the mechanism by which it operates. a) The Ekman spiral model. b) A body of water can be thought as a set of layers. The top layer is driven forward by the wind, and each layer below is moved by friction. Each succeeding layer moves at a slower speed, and at an angle to the layer immediately above it (to the right in the Northern Hemisphere, to the left in the Southern Hemisphere) until friction becomes negligible. (c) Though the direction of movement is different for each layer in the stack, the theoretical average direction of flow of water in the Northern Hemisphere is $90°$ to the right of the prevailing surface wind (Garrison, 1993).

5.1.3 Ekman spiral*

The Ekman spiral is a consequence of the Coriolis effect. When surface water molecules move by the force of the wind, they, in turn, drag deeper layers of water molecules below them. Each layer of water molecules is moved by friction from the shallower layer, and each deeper layer moves more slowly than the layer above it, until the movement ceases at a depth of about 100 meters. Like the surface water, however, the deeper water is deflected by the Coriolis effect-to the right in the Northern Hemisphere and to the left in the Southern Hemisphere. As a result, each successively deeper layer of water moves more slowly to the right or left, creating a spiral effect (Fig. 5.4). Because the deeper layers of water move more slowly than the shallower layers, they tend to "twist around" and flow not in the direction of the surface current.

Ekman developed the theory of the Ekman layer after Fridtjof Nansen observed that ice drifts at an angle of $20 - 40°$ to the right of the prevailing wind direction while on an Arctic expedition aboard the Fram. Nansen asked his colleague, Vilhelm Bjerknes to set one of his students upon study of the problem. Bjerknes tapped Ekman, who presented his results in 1902 as his doctoral thesis.

The mathematical formulation of the Ekman layer can be found by assuming a neutrally stratified fluid, with horizontal momentum in balance between the forces of pressure gradient, Coriolis and turbulent drag.

$$-fv = -\frac{1}{\rho_o}\frac{\partial}{\partial x}p + \nu\frac{\partial^2 u}{\partial z^2}, \tag{5.37}$$

$$fu = -\frac{1}{\rho_o}\frac{\partial}{\partial y}p + \nu\frac{\partial^2 v}{\partial z^2}, \tag{5.38}$$

where ν is the diffusive eddy viscosity, which can be derived using mixing length theory. There are many regions where an Ekman layer is theoretically plausible; they include the bottom of the atmosphere, near the surface of the earth and ocean, the bottom of the ocean, near the sea floor and at the top of the ocean, near the air-water interface. Different boundary conditions are appropriate for each of these different situations. We will consider boundary conditions of the Ekman layer in the upper ocean:

$$\text{at} \quad z = 0: \quad \nu\frac{\partial u}{\partial z} = \tau^x \quad \text{and} \quad \nu\frac{\partial v}{\partial z} = \tau^y, \tag{5.39}$$

where τ^x and τ^y are the components of the surface stress, τ, of the wind field or ice layer at the top of the ocean and u_g and v_g are the geostrophic flows as $z \to \infty : u \to u_g, v \to v_g$. In the other situations, other boundary conditions, such as the no-slip condition, may be appropriate instead.

The dynamics (5.37, 5.38) can be reformulated as

$$-fv = -fv_g + \nu\frac{\partial^2 u}{\partial z^2}, \tag{5.40}$$

$$fu = fu_g + \nu\frac{\partial^2 v}{\partial z^2}, \tag{5.41}$$

Now multiply (5.40) with i and subtract it from (5.41):

$$ifv - ifv_g + i\nu\frac{\partial^2 u}{\partial z^2} + fu - fu_g - \nu\frac{\partial^2 v}{\partial z^2} = 0 \tag{5.42}$$

Denoting $\xi = u + iv$, we get

$$f\xi - f\xi_g + i\nu\frac{\partial^2 \xi}{\partial z^2} = 0 \tag{5.43}$$

We rewite this as

$$\frac{\partial^2 \xi}{\partial z^2} - \left(\frac{if}{\nu}\right)\xi = -\left(\frac{if}{\nu}\right)\xi_g \tag{5.44}$$

We solve the inhomogenous equation (5.44) in two steps:

1. find a particular solution of the inhomogenous equation:

assume that ξ is independent on z

$$-\left(\frac{if}{\nu}\right)\xi = -\left(\frac{if}{\nu}\right)\xi_g \tag{5.45}$$

with the solution $\xi = \xi_g$

2. find a complementary function, a general solution of the homogenous part of (5.44):

$$\frac{\partial^2 \xi_h}{\partial z^2} - \left(\frac{if}{\nu}\right)\xi_h = 0 \tag{5.46}$$

$$\xi_h = C\exp(\lambda z) \quad \text{with} \quad \lambda^2 = \frac{if}{\nu} \tag{5.47}$$

Thus $$\lambda_\pm = \pm\frac{1+i}{\sqrt{2}}\sqrt{\frac{f}{\nu}} = \pm(1+i)\sqrt{\frac{f}{2\nu}} = \pm(1+i)\,\gamma \qquad (5.48)$$

Therefore

$$\xi_h = C_1\exp(\lambda_+ z) + C_2\exp(\lambda_- z) = C_1\exp(\gamma z)\exp(i\gamma z) + C_2\exp(-\gamma z)\exp(-i\gamma z)$$

As boundary condition ξ_h has to go to zero for $z\to\infty$, therefore $C_1 = 0$.

3. The complete solution is

$$\xi = \xi_g + C_2\exp(-\gamma z)\exp(-i\gamma z) \qquad (5.49)$$

As boundary condition $$\xi(z = 0) = 0 = \xi_g + C_2 \qquad (5.50)$$

Therefore $$\xi = \xi_g \cdot (1 - \exp(-\gamma z)\exp(-i\gamma z)) \qquad (5.51)$$

For simplicity, we can assume that the geostrophic flow is zonal, so that $v_g = 0$. Then,

$$u = u_g \cdot (1 - \exp(-\gamma z)\cos(\gamma z)) \qquad (5.52)$$

$$v = u_g \cdot (\exp(-\gamma z)\sin(\gamma z)) \qquad (5.53)$$

This variation of horizontal velocity with depth (-z) is referred to as the Ekman spiral, diagrammed above (Fig. 5.4). If we make a Taylor expansion for small z, we see that

$$u = u_g \cdot \gamma z \qquad (5.54)$$

$$v = u_g \cdot \gamma z \qquad (5.55)$$

Thus the low is $45°$ to the left of the limiting zonal gestrophic flow.

By applying the continuity equation we can have the vertical velocity as following

$$w = \frac{1}{f\rho_o} \left[\left(\frac{\partial \tau^y}{\partial x} - \frac{\partial \tau^x}{\partial y} \right) \left(1 - e^{-\gamma z} \cos{(\gamma z)}\right) - \left(\frac{\partial \tau^x}{\partial x} + \frac{\partial \tau^y}{\partial y} \right) e^{-\gamma z} \sin{(\gamma z)} \right]$$

Note that when vertically integrated the volume transport associated with the Ekman spiral is to the right of the wind direction in the Northern Hemisphere.

There is much difficulty associated with observing the Ekman layer for two main reasons: the theory is too simplistic as it assumes a constant eddy viscosity, which Ekman himself anticipated, recognizing that is obvious that ν cannot generally be regarded as a constant when the density of water is not uniform within the region considered and because it is difficult to design instruments with great enough sensitivity to observe the velocity profile in the ocean.

Because the real ocean does not match the idealized conditions of the Ekman spiral, wind-induced water movements often differ appreciably from theoretical predictions. In shallow water, for example, the water depth is insufficient for the full spiral to develop so that the angle between the horizontal wind direction and surface-water movements can be as little as 15 degrees. As waters deepen, the angle increases and approaches 45 degrees. The stable pycnocline inhibits the transfer of kinetic energy to deeper waters, helping to contain wind-driven currents to the mixed layer; that is, the pycnocline acts as a permeable boundary for Ekman transport and surface currents.

Exercise 39   –   Ekman layer in the atmosphere

Consider a geostrophic flow (u_g, v_g)

$$-fv_g = -\frac{1}{\rho_0}\frac{\partial p}{\partial x} \tag{5.56}$$

$$fu_g = -\frac{1}{\rho_0}\frac{\partial p}{\partial y} \quad . \tag{5.57}$$

The boundary-layer equations are then

$$-f(v - v_g) = \nu \frac{\partial^2 u}{\partial z^2} \tag{5.58}$$

$$f(u - u_g) = \nu \frac{\partial^2 v}{\partial z^2} \quad . \tag{5.59}$$

The boundary conditions are specified to be at the surface

$$\rho_0 \nu \frac{\partial u}{\partial z} = \tau^x \tag{5.60}$$

$$\rho_0 \nu \frac{\partial v}{\partial z} = \tau^y \tag{5.61}$$

and for $z \to -\infty : u = u_g, \quad v = v_g$.

1. Calculate the flow (u,v) as the departure from the interior flow (u_g, v_g)!

2. Calculate the net wind-driven horizontal transport through integration

$$V = \int_{-\infty}^{0} dz(v - v_g) \quad \text{and} \quad U = \int_{-\infty}^{0} dz(u - u_g) \quad . \tag{5.62}$$

What is the direction of U and V in terms of the surface wind stress τ?

3. For the case $f = f_0$ of constant Coriolis parameter, determine the divergence of the flow

$$\int_{-\infty}^{0} dz \left(\frac{\partial u}{\partial x} + \frac{\partial v}{\partial y} \right) \tag{5.63}$$

which is identical to the vertical velocity across the Ekman layer (since w(0)=0).

Exercise 40   –   Ekamn spiral in the ocean

Consider the solution (5.52,5.53) for the wind-driven Ekman layer at the surface of the ocean in the Northern Hemisphere. The geostrophic velocity is zero in this example. Show that (5.52,5.53) is a solution of (5.37, 5.38) !

5.1.4   Tea leaf paradox*

The tea leaf paradox describes a phenomenon where tea leaves in a cup of tea migrate to the center and bottom of the cup after being stirred rather than being forced to the edges of the cup, as would be expected in a spiral centrifuge.[3] Stirring the liquid makes it spin around the cup. Because of inertia, the pressure is higher along the rim than in the middle. However, near the bottom and outer edges the liquid is slowed by the friction against the cup. There the outward force cannot overcome the pressure gradient, so these pressure differences become more important for the water flow. This is called a boundary layer or more specifically an Ekman layer.

In a teacup, where the rotation is slower at the bottom, the pressure gradient takes over and creates an inward flow along the bottom. Higher up, the liquid flows outward instead. This secondary flow travels inward along the bottom bringing the leaves to the center, then up, out and down near the rim. The leaves are too heavy to lift upwards, so they stay in the middle. Combined with the primary rotational flow, the leaves will spiral inward along the bottom.

Besides tea leaves stirred in a cup, other classroom demonstrations can show the secondary circulation that arises due to the presence of friction. We discuss a simple laboratory experiment below, which demonstrates these ideas in a more controlled setting and can be readily applied to both atmospheric low and high pressure systems. All one needs is a rotating turntable, a cylindrical container (a large transparent beaker or a cylindrical insert inside a square container works fine), and some potassium permanganate crystals. When rotated at a constant rate, all the water comes

---

[3]The formation of secondary flows in an annular channel was theoretically treated by Boussinesq in 1868.The migration of near-bottom particles in river-bend flows was experimentally investigated by A.Ya.Milovich in 1913. The solution first came from Albert Einstein in a 1926 paper where he used it to explain the erosion of river banks (Baer's law) [Einstein, 1926].
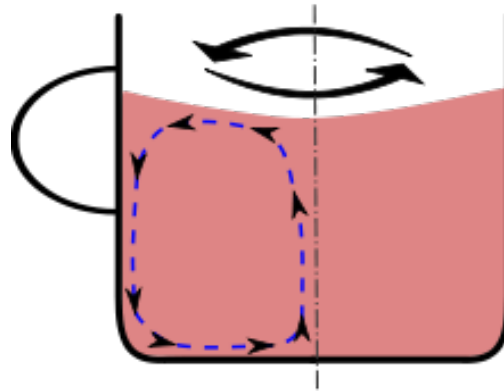
Figure 5.5:   The blue line is the secondary flow that pushes the tea leaves to the middle of the bottom.

into solid body rotation, and so there is no Coriolis or centrifugal accelerations acting. The key experimental requirement is to be able to speed up or slow down (by 10% or so) the rate of rotation of the turntable so as to induce relative motion between the water and the tank, thus creating a frictional boundary layer. The rotating platform can be used in a whole series of experiments to demonstrate atmospheric and oceanic phenomena, as presented in Marshall and Plumb (2007) and their "Weather in a Tank" website.

A tank of water is placed on the rotating platform long enough for water to reach solid body rotation, say, about 10 minutes for 10-15 rpm. Then we drop a very few potassium permanganate crystals in an equilateral triangle about the center. This shows up as three small clouds when viewed by a rotating camera. We also drop a few colored paper dots on the surface to see the flow outside the boundary layer. As the table is slowed down by a few rpm (about 10%), the permanganate on the bottom traces the near bottom circulation, which is cyclonic and inward, just like a low pressure system. The paper dots floating on the surface do not go inward. Why does this happen?

The water outside the boundary layer is still rotating with the original fast rotation rate, while the water at the bottom is rotating slower, at the new slower rotation rate. This speed differential, just like the low pressure system leads to an inward flow which is seen in the permanganate streaks

Figure 5.6: To carry out the experiment we first very slightly reduce (by 10% max) the rate of rotation of the turntable. Because of the inertia of the turning fluid, it continues to spin at its original speed and so moves relative to the tank: permanganate streaks are pulled around not in circles as one might initially expect, but rather inward turning, anticlockwise spirals, as can be seen in the top panel. A beautiful symmetric pattern is remarkably easy to achieve. This is analogous to the near-surface flow in a low pressure system, as can be seen by comparing with Fig. 1.2 (see low pressure system). To visualize the flow at the upper surface, we can float a few paper dots on the surface (black dots are the most visible in this application). We observe circular, rather than spiraling, motion. To create an analogy of a high pressure system we now simply increase the speed of the turntable by 10% or so (back up to, roughly, its original speed). We observe the dye streaks on the bottom reversing and, over time, spiraling clockwise and outwards, as can be seen in the lower panel in this figure. This should be compared to the pattern of surface winds that can be seen in the high pressure system in Fig. 1.2. From Marshall and Plumb (2007).

at the bottom (Fig. 5.6). Similarly, the pressure gradient can be reversed by increasing the speed by a few rpm to the original speed, and it leads to permanganate streaks that show an outward anti-cyclonic flow, analogous to the surface boundary layer of a High pressure system. This secondary flow in the boundary layer has important implications for movement in the vertical direction. The inward flow associated with a low pressure system leads to rising air near the center of the Low. As this air rises, it expands (pressure always decreases going upward in the atmosphere) and cools. Since the saturation of the air is very strongly dependent on the temperature, as the air cools, it may get saturated, and the water vapor may condense out to form clouds! This is why the Low pressure systems are the ones associated with stormy weather and precipitation. Conversely, high pressure systems are associated with outward motion in the boundary layer, and hence subsidence. As the air descends, it gets compressed due to the pressure increase, warms, and becomes less and less saturated. Thus the High pressure systems are fair weather systems.
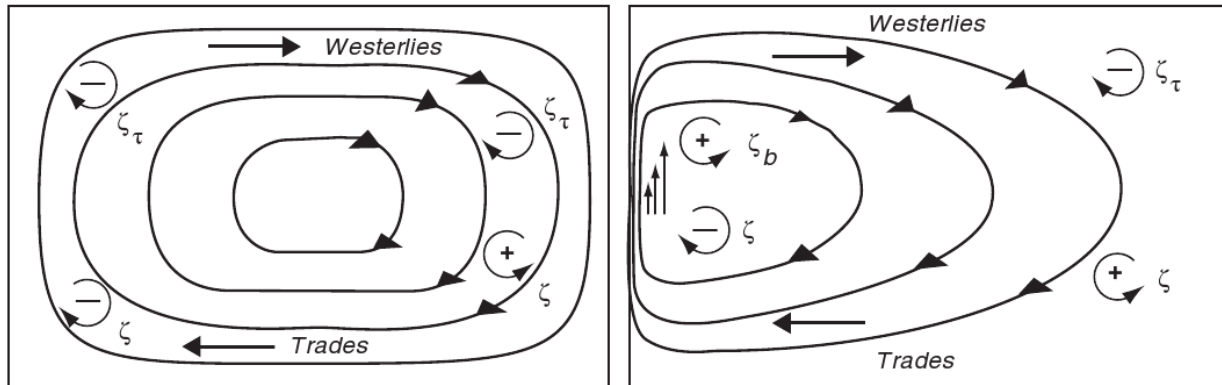
Figure 5.7: The balance of potential vorticity can clarify why western boundary currents are necessary. **Left**: Vorticity input by the wind ζ_τ balances the change in relative vorticity ζ in the east as the flow moves southward and f decreases. The two do not balance in the west where ζ must decrease as the flow moves northward and f increases. **Right**: Vorticity in the west is balanced by relative vorticity ζ_b generated by shear in the western boundary current.

5.1.5 Western Boundary Currents

The balance of vorticity provides an alternative explanation for the existence of western boundary currents. Consider the gyrescale flow in an ocean basin (Fig. 5.7), say in the North Atlantic from $10°$N to $50°$N. The wind blowing over the Atlantic adds negative vorticity ζ_τ. As the water flows around the gyre, the vorticity of the gyre must remain nearly constant, else the flow would spin faster or slower. Overall, the negative vorticity input by the wind must be balanced by a source of positive vorticity.

Throughout most of the basin the negative vorticity input by the wind is balanced by an increase in relative vorticity. As the flow moves southward throughout the basin, f decreases and ζ must increase according to (3.64) because the depth of the wind-driven circulation does not change much.

The balance breaks down, however, in the west where the flow returns northward. In the west, f increases, ζ decreases, and a source of positive vorticity is needed. The positive vorticity ζ_b is produced by the western boundary boundary current.

Stommel's Theory of Western Boundary Currents

At the same time Sverdrup was beginning to understand circulation in the eastern Pacific, Stommel was beginning to understand why western boundary currents occur in ocean basins. To study the circulation in the north Atlantic, Stommel (1948) used essentially the same equations used by Sverdrup (5.11, 5.12, 5.13, 5.14, 5.15 and 5.16) but he added a bottom stress proportional to velocity to (5.15) and (5.16):

$$\left(A_z \frac{\partial u}{\partial z}\right)_0 = -\tau_x = -F \cos\left(\pi \, y/b\right) \qquad \left(A_z \frac{\partial u}{\partial z}\right)_D = -R \, u \qquad (5.64)$$

$$\left(A_z \frac{\partial v}{\partial z}\right)_0 = -\tau_y = 0 \qquad \left(A_z \frac{\partial v}{\partial z}\right)_D = -R \, v \qquad (5.65)$$

where F and R are constants.

Stommel calculated steady-state solutions for flow in a rectangular basin $0 \leq y \leq b$, $0 \leq x \leq \lambda$ of constant depth D filled with water of constant density. His first solution was for a non-rotating Earth. This solution had a symmetric flow pattern with no western boundary current (Fig. 5.8, left). Next, Stommel assumed a constant rotation, which again led to a symmetric solution with no western boundary current. Finally, he assumed that the Coriolis force varies with latitude. This led to a solution with western intensification (Fig. 5.8, right).

Exercise 41   –   The Stommel model of the wind-driven circulation

The wind-driven circulation in a homogeneous ocean of constant depth h is described by

$$R\nabla^2\psi + \beta\partial_x\psi \;=\; \mathrm{curl}(\tau/\rho_0) \qquad (5.66)$$

$$\;=\; (\partial_x\tau^y - \partial_y\tau^x)/\rho_0 \qquad (5.67)$$

where R is a coefficient of bottom friction, β the derivative of the Coriolis frequency at a central latitude, and the τ the windstress vector. Finally, ψ is the streamfunction of the depth integrated
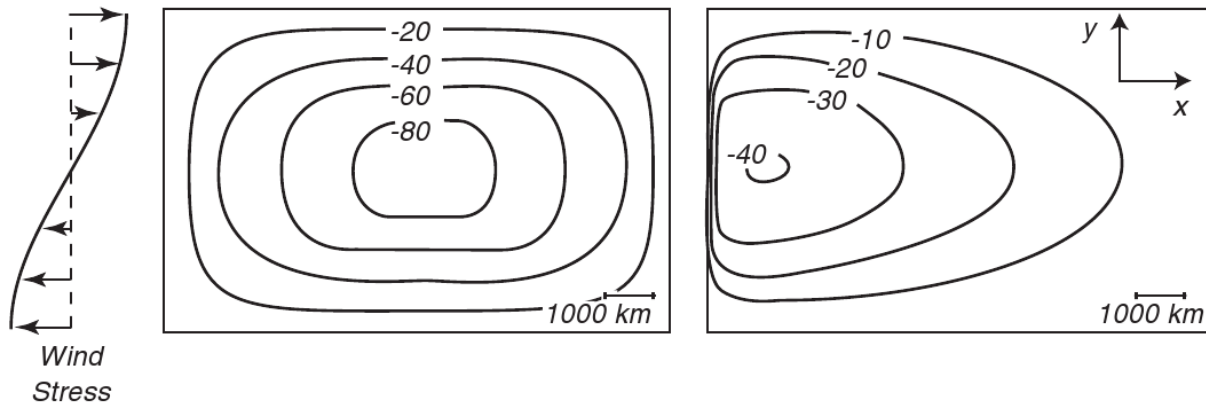
Figure 5.8: Stream function for flow in a basin as calculated by Stommel (1948). Left: Flow for non-rotating basin or flow for a basin with constant rotation. Right: Flow when rotation varies linearly with y.

velocity

$$U = (U, V) = \int_{-h}^{0} u\,dz$$

i.e.

$$U = -\partial_y \psi, \quad V = \partial_x \psi$$

1. Derive this equation from the conservation of momentum (linearized) and mass (volume!) assuming $w = 0$ at the mean surface $z = 0$ and at the bottom $z = -h$. For simplicity take Cartesian coordinates for the horizontal, $\beta = df/dy$. Boundary condition for the flux of momentum are $\tau(z = 0) = \tau$ and $\tau(z = -h) = R(-V, U)$. Hint: integrate both equations vertically and take the curl of the integrated momentum balance.

2. in the boundary layer the terms on the left hand side of (5.66) get large. Show by scaling that the width of the layer is $W = R/\beta$.

3. how large must R be to get a width $W = 100$ km? ($\beta = 2 \times 10^{-11}$ m^{-1}s^{-1}).

Munk's Solution

Sverdrup's and Stommel's work suggested the dominant processes producing a basin-wide, wind-driven circulation. Munk (1950) built upon this foundation, adding information from Rossby (1936) on lateral eddy viscosity, to obtain a solution for the circulation within an ocean basin. Munk used Sverdrup's idea of a vertically integrated mass transport flowing over a motionless deeper layer. This simplified the mathematical problem, and it is more realistic. The ocean currents are concentrated in the upper kilometer of the ocean, they are not barotropic and independent of depth. To include friction, Munk used lateral eddy friction with constant $A_H = A_x = A_y$. Equations (5.11) (5.12) become:

$$\frac{1}{\rho}\frac{\partial p}{\partial x} = \quad f\,v + \frac{\partial}{\partial z}\left(A_z\frac{\partial u}{\partial z}\right) + A_H\frac{\partial^2 u}{\partial x^2} + A_H\frac{\partial^2 u}{\partial y^2} \tag{5.68}$$

$$\frac{1}{\rho}\frac{\partial p}{\partial y} = \;-\; f\,u + \frac{\partial}{\partial z}\left(A_z\frac{\partial v}{\partial z}\right) + A_H\frac{\partial^2 v}{\partial x^2} + A_H\frac{\partial^2 v}{\partial y^2} \tag{5.69}$$

Munk integrated the equations from a depth $-D$ to the surface at $z = z_0$ which is similar to Sverdrup's integration except that the surface is not at $z = 0$. Munk assumed that currents at the depth $-D$ vanish, that (5.15) and (5.16) apply at the horizontal boundaries at the top and bottom of the layer, and that A_H is constant. To simplify the equations, Munk used the mass-transport stream function (3.47), and eliminated the pressure term by taking the y derivative of (5.68) and the x derivative of (5.69):

$$\underbrace{A_H\nabla^4\Psi}_{\text{Friction}} - \underbrace{\beta\frac{\partial\Psi}{\partial x} = -\,\text{curl}_z\,\tau}_{\text{Sverdrup Balance}} \tag{5.70}$$

where

$$\nabla^4 = \frac{\partial^4}{\partial x^4} + 2\frac{\partial^4}{\partial x^2\,\partial y^2} + \frac{\partial^4}{\partial y^4} \tag{5.71}$$

is the biharmonic operator. Equation (5.70) is the same as (5.20) with the addition of the lateral friction term A_H. The friction term is large close to a lateral boundary where the horizontal derivatives of the velocity field are large, and it is small in the interior of the ocean basin. Thus in

the interior, the balance of forces is the same as that in Sverdrup's solution.

Equation (5.70) is a fourth-order partial differential equation, and four boundary conditions are needed. Munk assumed the flow at a boundary is parallel to a boundary and that there is no slip at the boundary:

$$\Psi_{\text{boundary}} = 0, \qquad \left(\frac{\partial \Psi}{\partial n}\right)_{\text{boundary}} = 0 \tag{5.72}$$

where n is normal to the boundary. Munk then solved (5.70) with (5.72) assuming the flow was in a rectangular basin extending from $x = 0$ to $x = r$, and from $y = -s$ to $y = +s$. He further assumed that the wind stress was zonal and in the form:

$$\tau = a \cos ny + b \sin ny + c \tag{5.73}$$

$$n = j \, \pi/s, \qquad j = 1, 2, \dots \tag{5.74}$$

Munk's solution (figure 5.9) shows the dominant features of the gyre-scale circulation in an ocean basin. It has a circulation similar to Sverdrup's in the eastern parts of the ocean basin and a strong western boundary current in the west. Using $A_H = 5 \cdot 10^3 \frac{m^2}{s}$ gives a boundary current roughly $225km$ wide with a shape similar to the flow observed in the Gulf Stream and the Kuroshio.

The transport in western boundary currents is independent of A_H, and it depends only on (5.20) integrated across the width of the ocean basin. Hence, it depends on the width of the ocean, the curl of the wind stress, and β. Using the best available estimates of the wind stress, Munk calculated that the Gulf Stream should have a transport of $36Sv$ and that the Kuroshio should have a transport of $39Sv$. The values are about one half of the measured values of the flow available to Munk. This is very good agreement considering the wind stress was not well known.[4]

---

[4]Recent recalculations show good agreement except for the region offshore of Cape Hatteras where there is a strong recirculation. Munk's solution was based on wind stress averaged over $5°$ squares. This underestimated the curl of the stress. Leetmaa and Bunker (1978) used modern drag coefficient and $2° \times 5°$ averages of stress to obtain $32Sv$ transport in the Gulf Stream, a value very close to that calculated by Munk.
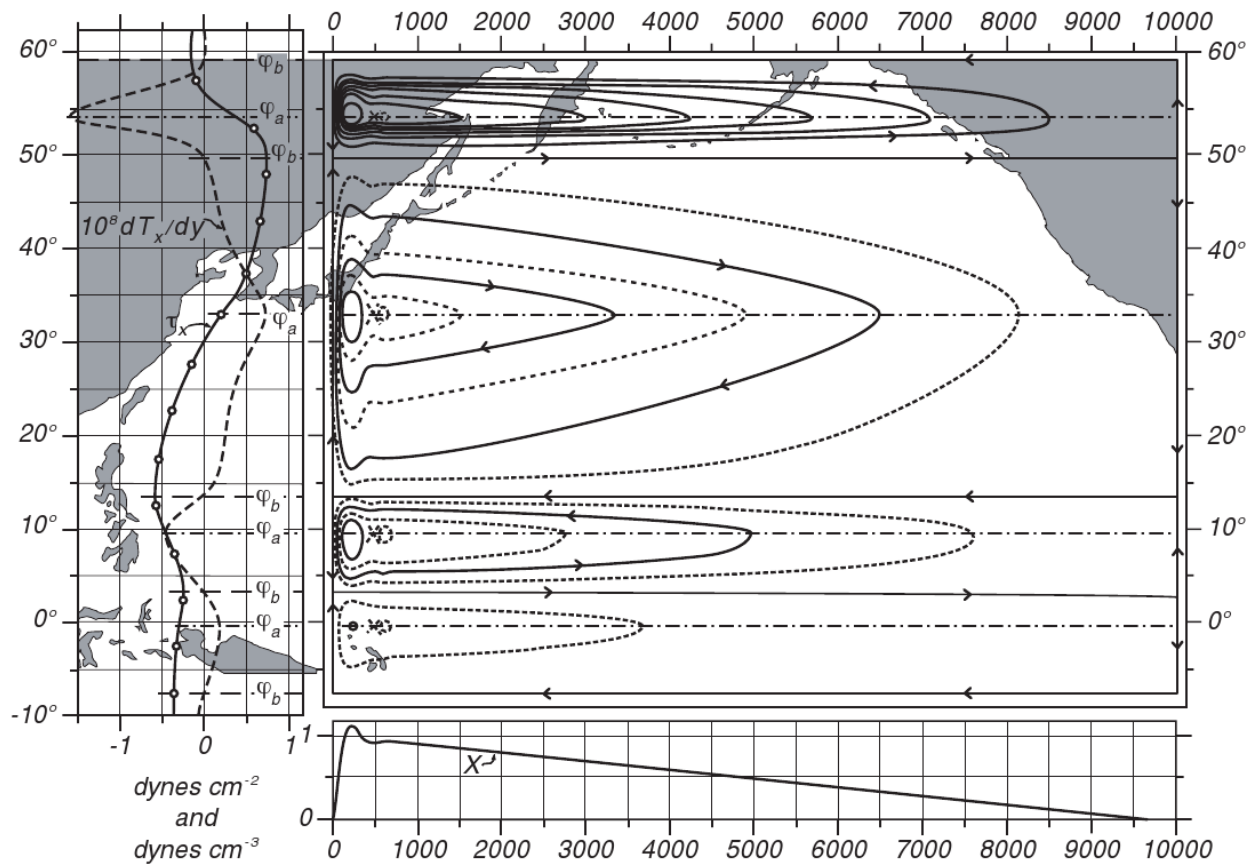
Figure 5.9: **Left**: Mean annual wind stress $\tau_x(y)$ over the Pacific and the curl of the wind stress. ϕ_b are the northern and southern boundaries of the gyres, where $M_y = 0$ and $\mathbf{curl}\,\tau = 0$. ϕ_0 is the center of the gyre. **Upper Right**: The mass transport stream function for a rectangular basin calculated by Munk (1950) using observed wind stress for the Pacific. Contour interval is **10** Sverdrups. The total transport between the coast and any point x, y is $\psi(x,y)$. The transport in the relatively narrow northern section is greatly exaggerated. **Lower Right**: North-South component of the mass transport. After Munk (1950).

Summarizing important concepts of vorticity

- Vorticity strongly constrains ocean dynamics

- Vorticity due to earth's rotation is much greater than other sources of vorticity

- Taylor and Proudman showed that vertical velocity is impossible in a uniformly rotating flow. Hence Ekman pumping requires that planetary vorticity varies with latitude.

- The curl of the wind stress adds relative vorticity to central gyres of each ocean basin. For steady state circulation in the gyre, the ocean must lose vorticity in western boundary currents.

- Positive wind stress curl leads to divergent flow in the Ekman layer. The ocean's interior geostrophic circulation adjusts through a northward mass transport.

Exercise 42 – Cyclostrophic wind

When the flow is sufficiently near the equator so that f is small or when the Corolis force is negligible compared to the centripedal acceleration, the gradient wind equation becomes

$$\frac{v\mathbf{k} \times \mathbf{v}}{R} = -\frac{1}{\rho}\nabla_z p \tag{5.75}$$

where $\mathbf{k}$ is the unit vector in z direction, $\mathbf{v}$ is the velocity vector, v ist the meridional velocity, R Earth radius, ∇_z horizontal nabla operator.

1. Derive this equation!
2. What is the associated gradient wind equation including the Coriolis force?
3. What is the Rossby number?

Part III

Third part: Stochastic climate model and Mesoscopic Dynamics

Part IV

Fourth part: Programming and tools

Bibliography

Abramowitz, M. and Stegun, I. A. (1965). Handbook of mathematical functions with formulas, graph, and mathematical tables. *Applied Mathematics Series*, 55:1046.

Arnold, L. (1995). *Random dynamical systems*. Springer.

Arnold, L. (2001). *Hasselmann's program revisited: The analysis of stochasticity in deterministic climate models*, volume 49. Birkhäuser, Boston.

Baker, G. L. and Blackburn, J. A. (2005). *The pendulum: a case study in physics*, volume 8. Oxford University Press Oxford.

Barber, D., Dyke, A., Hillaire-Marcel, C., Jennings, J., Andrews, J., Kerwin, M., Bilodeau, G., McNeely, R., Southon, J., Morehead, M., and Gagnonk, J.-M. (1999). Forcing of the cold event of 8,200 years ago by catastrophic drainage of laurentide lakes. *Nature*, 400(6742):344–348.

Bhatnagar, P., Gross, E. P., and Krook, M. K. (1954). A model for collision process in gases. i. small amplitude processes in charged and neutral one-component system. *Phys. Rev*, 94:511.

Boltzmann, L. (1896). *Vorlesungen über Gastheorie : 2 Volumes (in German)*. Leipzig 1895/98 UB: O 5262-6.

Boltzmann, L. (1995). *Lectures on Gas Theory*. Dover Publ. New York. ISBN 978-0486684550.

Broecker, S. and Peng, T.-H. (1982). *Tracers in the Sea*. Columbia University.

Broecker, W. S. (1987). The biggest chill. *Natural History*, 97(2):74–82.

Broecker, W. S. et al. (1991). The great ocean conveyor. *Oceanography*, 4(2):79–89.

Brüning, R. and Lohmann, G. (1999). Charles s. peirce on creative metaphor: a case study on the conveyor belt metaphor in oceanography. *Foundations of science*, 4(4):389–403.

Bryan, F. (1986). High latitude salinity effects and inter-hemispheric thermohaline circulations. *Nature*, 323(3):301–304.

Buckingham, E. (1914). On physically similar systems; illustrations of the use of dimensional equations. *Physical Review*, 4(4):345–376.

Budyko, M. I. (1969). The effect of solar radiation variations on the climate of earth. *Tellus*, 21:611–619.

Busch, W. (1865). *Max und Moritz (in German); Max and Maurice, a Juvenile History in Seven Tricks* . Braun und Schneider, München.

Cercignani, C. (1987). *The Boltzmann equation and its applications*. Springer New York. ISBN 978-0387966373.

Cercignani, C. (1990). *Mathematical methods in kinetic theory*. Plenum, 2 edition. ISBN 978-0306434600.

Chelton, D. B. and Schlax, M. G. (1996). Global Observations of Oceanic Rossby Waves. *Science*, 272:234–238.

Chen, D., Gerdes, R., and Lohmann, G. (1995). A 1-d atmospheric energy balance model developed for ocean modelling. *Theoretical and Applied Climatology*, 51:25–38.

Chorin, A. J. and Hald, O. H. (2006). Stochastic tools in mathematics and science. surveys and tutorials in the applied mathematical sciences, vol. 1.

Chorin, A. J., Kast, A. P., and Kupferman, R. (1999). Unresolved computation and optimal predictions. *Communications on pure and applied mathematics*, 52(10):1231–1254.

Chorin, A. J., Kupferman, R., and Levy, D. (2000). Optimal prediction for hamiltonian partial differential equations. *Journal of Computational Physics*, 162(1):267–297.

Courant, R., Friedrichs, K., and Lewy, H. (1928). Über die partiellen Differenzengleichungen der mathematischen Physik. *Mathematische Annalen*, 100:32–74.

Courant, R., Friedrichs, K., and Lewy, H. (1967). On the partial difference equations of mathematical physics. *IBM J. Res. Dev.*, 11(2):215–234.

Dansgaard, W., Johnsen, S., Clausen, H., Dahl-Jensen, D., Gundestrup, N., Hammer, C., C.S. Hvidberg, J. S., Sveinbjoernsdottir, A., Jouzel, J., and Bond, G. (1993). Evidence for general instability of past climate from a 250-kyr ice-core record. *Nature*, 364:218–220.

d'Humieres, D., Bouzidi, M., and Lallemand, P. (2001). Thirteen-velocity three-dimensional lattice boltzmann model. *PRE*, 63(6, Part 2).

Dijkstra, H., Raa, L. T., and Weijer, W. (2004). A systematic approach to determine thresholds of the ocean's thermohaline circulation. *Tellus A*, 56 (4):362.

Doedel, E. J., Champneys, A. R., Fairgrieve, T. F., Kuznetsov, Y. A., Sandstede, B., and Wang, X. (1997). Continuation and bifurcation software for ordinary differential equations (with homcont). *Available by anonymous ftp from ftp cs concordia ca, directory pub/doedel/auto*.

Egger, J. (2001). Master equations for climatic parameter sets. *Climate Dynamics*, 18(1-2):169–177.

Einstein, A. (1905). Investigations on the theory of the brownian movement. *Ann. der Physik*, 17:549–560.

Einstein, A. (1926). Die Ursache der Mäanderbildung der Flußläufe und des sogenannten Baerschen Gesetzes. *Naturwissenschaften*, 14:223–224.

Evans, D. J. and Morriss, G. (2008). *Statistical mechanics of nonequilibrium liquids*. Cambridge University Press.

Fairbanks, R. G. (1989). A 17, 000-year glacio-eustatic sea level record: influence of glacial melting rates on the younger dryas event and deep-ocean circulation. *Nature*, 342(6250):637–642.

Feigenbaum, M. J. (1980). The transition to aperiodic behaviour in turbulent systems. *Commun. Math. Phys.*, 77.

Flammer, C. (1957). *Spheroidal wave functions*. Stanford University Press.

Frisch, U. (1996). *Turbulence: the legacy of A.N. Kolmogorov*. Cambridge University Press. ISBN 0-521-45103-5.

Gerkema, T., Zimmerman, J., Maas, L., and Van Haren, H. (2008). Geophysical and astrophysical fluid dynamics beyond the traditional approximation. *Reviews of Geophysics*, 46(2).

Gill, A. E. (1982). *Atmosphere-ocean dynamics*, volume 30. Academic Press. International Geophysics Series.

Givon, D., Kupferman, R., and Stuart, A. (2004). Extracting macroscopic dynamics: model problems and algorithms. *Nonlinearity*, 17(6):R55.

Gottwald, G. (2010). On recent trends in climate dynamics. *AMS Gazette*, 37(5).

Grassberger, P. and Procaccia, I. (1983). Measuring the strangeness of strange attractors. *Physica D: Nonlinear Phenomena*, 9(2):189–208.

Haken, H. (1996). Slaving principle revisited. *Physica D: Nonlinear Phenomena*, 97(1):95–103.

Haney, R. L. (1971). Surface thermal boundary conditions for ocean circulation models. *Journal of Physical Oceanography*, 1:241–248.

Hasselmann, K. (1976). Stochastic climate models. Part I. Theory. *Tellus*, 6:473–485.

He, X. and Luo, L. S. (1997). Theory of the lattice Boltzmann method: From the Boltzmann equation to the lattice Boltzmann equation. *Phys. Rev. E*, 56(6):6811–6817.

Holton, J. R. (2004). *An Introduction to Dynamic Meteorology*. Elsevier Academic Press, Burlington, MA.

Kambe, T. (2007). *Elementary Fluid Mechanics*. World Scientific Publishing.

Kuznetsov, Y. A. (1998). *Elements of applied bifurcation theory*, volume 112. Springer, New York.

Landau, L. D. and Lifshitz, E. M. (1959). *Fluid Mechanics*, volume 6 of *Course of Theoretical Physics*. Pergamon Press, Oxford.

Langevin, P. (1908). On the theory of brownian motion. *Comptes Rendues*, 146:530–533.

Leith, C. (1975). Climate response and fluctuation dissipation. *Journal of the Atmospheric Sciences*, 32(10):2022–2026.

Lohmann, G. (2003). Atmospheric and oceanic freshwater transport during weak atlantic overturning circulation. *Tellus A*, 55(5):438–449.

Longuet-Higgins, M. S. (1968). The eigenfunctions of laplace's tidal equations over a sphere. *Philosophical Transactions for the Royal Society of London. Series A, Mathematical and Physical Sciences*, pages 511–607.

Lorenz, E. (1982). Atmospheric predictability experiments with a large numerical model. *Tellus A*, 34:505–513.

Lorenz, E. N. (1960). Maximum simplification of the dynamic equations. *Tellus*, 12(3):243–254.

Lorenz, E. N. (1963). Deterministic nonperiodic flow. *Journal of the atmospheric sciences*, 20(2):130–141.

Lorenz, E. N. (1976). Nondeterministic theories of climatic change. *Quaternary Research*, 6(4):495–506.

Lorenz, E. N. (1984). Irregularity: a fundamental property of the atmosphere*. *Tellus A*, 36(2):98–110.

Lucarini, V., Blender, R., Herbert, C., Pascale, S., Ragone, F., and Wouters, J. (2014). Mathematical and physical ideas for climate science. *Rev. Gephys.*

Maas, L. R. (1994). A simple model for the three-dimensional, thermally and wind-driven ocean circulation. *Tellus A*, 46(5):671–680.

Manabe, S. and Stouffer, R. (1993). Century-scale effects of increased atmospheric CO_2 on the ocean atmosphere system. *Nature*, 364:215–218.

Mandelbrot, B. B. (1967). How long is the coast of britain: Statistical self-similarity and fractal dimension. *Science*, 155:636–638.

Mandelbrot, B. B. (1983). *The fractal geometry of nature*. Macmillan.

Matsuno, T. (1966). Quasi-geostrophic motions in the equatorial area. *J. Meteor. Soc. Japan*, 44(1):25–43.

Mori, H. (1965). Transport, collective motion, and brownian motion. *Progress of Theoretical Physics*, 33(3):423–455.

Mori, H., Fujisaka, H., and Shigematsu, H. (1974). A new expansion of the master equation. *Progress of Theoretical Physics*, 51(1):109–122.

Müller and Maier-Reimer (2000). Trapped rossby waves. *Phys. Rev. E*, 61:1468 – 1485.

Müller, D., Kelly, B., and O'brien, J. (1994). Spheroidal eigenfunctions of the tidal equation. *Physical review letters*, 73(11):1557.

Müller, D. and O'Brien, J. (1995). Shallow water waves on the rotating sphere. *Physical Review E*, 51(5):4418.

Olbers, D. (2001). A gallery of simple models from climate physics. *In: Stochastic Climate Models, Progress in Probability (Eds.: P. Imkeller and J. von Storch)*, 49:3–63.

Peitgen, H.-O. and Richter, P. (1986). *The Beauty of Fractals*. Heidelberg: Springer-Verlag.

Proudman, J. (1916). On the motion of solids in a liquid possessing vorticity. *Proc. R. Soc. Lond. A*, 92:408–424.

Rahmstorf, S. (1996). On the freshwater forcing and transport of the Atlantic thermohaline circulation. *Climate Dynamics*, 12:799–811.

Rayleigh, L. (1916). On convection currents in a horizontal layber of fluid, when the higher temperature is on the under side. *Phil. Mag.*, 6:529–546.

Rooth, C. (1982). Hydrology and ocean circulation. *Progress in Oceanography*, 11:131–149.

Rossby, C.-G. (1939). "relation between variations in the intensity of the zonal circulation of the atmosphere and the displacements of the semi-permanent centers of action". *Journal of Marine Research*, 2 (1):38–55.

Saltzman, B. (1962). Finite amplitude free convection as an initial value problem – i. *Journal of the Atmoshpheric Sciences*, 19:329–341.

Shannon, C. E. (1948). A Mathematical Theory of Communication. *Bell System Technical Journal*, 27 (3):379–423.

Stommel, H. (1961). Thermohaline convection with two stable regimes of flow. *Tellus*, 13:224–230.

Strogatz, S. (2000). *Non-linear Dynamics and Chaos: With applications to Physics, Biology, Chemistry and Engineering*. Perseus Books.

Taylor, G. (1917). Motion of solids in fluids when the flow is not irrotational. *Proc. R. Soc. Lond. A*, 93:92–113.

Townsend, S., Lenosky, T., Muller, D., Nichols, C., and Elser, V. (1992). Negatively curved graphitic sheet model of amorphous carbon. *Physical Review Letters*, 69(6):921–924.

Tritton, D. J. (1988). *Physical Fluid Dynamics*. Oxford University Press, Science Publication. ISBN 978-0-19-854493-7.

Uhlenbeck, G. E. and Ornstein, L. S. (1930). On the theory of the brownian motion. *Physical review*, 36(5):823.

van Kampen, N. G. (1981). *Stochastic processes in physics and chemistry*. North Holland. IISBN 978-0-444-52965-7.

Wüst, G. (1935). Schichtung und Zirkulation des Atlantischen Ozeans. Das Bodenwasser und die Stratosphäre. *Wiss. Ergebn. Dtsch. Atlant. Exped. 'Meteor' 1925-1927*, 6(1):1–288.

Zwanzig, R. (1960). Ensemble method in the theory of irreversibility. *The Journal of Chemical Physics*, 33:1338.

Zwanzig, R. (1980). Problems in nonlinear transport theory. In *Systems far from equilibrium*, pages 198–225. Springer.

Zwanzig, R. (2001). *Nonequilibrium statistical mechanics*. Oxford University Press, USA.